E-cadherin endocytosis is modulated by p120-catenin through the opposing actions of RhoA and Arf1

Joshua Greig[1], Natalia A. Bulgakova[1, *]

[1] Department of Biomedical Science and Bateson Centre, The University of Sheffield, Sheffield S10 2TN, United Kingdom.

[*] Corresponding author: n.bulgakova@sheffield.ac.uk

Running title: E-cad turnover by p120ctn

Keywords: E-cadherin, p120-catenin, Arf1, RhoA, endocytosis, cell adhesion, clathrin

Wordcount: 6775

Abstract

The regulation of E-cadherin at the plasma membrane by endocytosis is of vital importance for developmental and disease. p120-catenin, which binds to the E-cadherin C-terminus, can both promote and inhibit E-cadherin endocytosis. However, little is known about what determines the directionality of p120-catenin activity, and the molecules downstream. Here, we have discovered that p120-catenin fine-tunes the clathrin-mediated endocytosis of E-cadherin in *Drosophila* embryonic epidermal cells. It simultaneously activated two actin-remodelling pathways with opposing effects: RhoA, which stabilized E-cadherin at the membrane, and Arf1, which promoted internalization. Epistasis experiments revealed that RhoA additionally inhibited Arf1. E-cadherin was efficiently endocytosed only in the presence of intermediate p120-catenin amounts with too little and too much p120-catenin inhibiting E-cadherin endocytosis. Finally, we found that p120-catenin levels altered the tension of the plasma membrane. Altogether, this shows that p120-catenin is a central hub which co-ordinates cell adhesion, endocytosis, and actin dynamics with tissue tension.

Introduction

Cell-cell adhesion is a fundamental requirement for the formation of tissues and organs. Such adhesions link cells to their neighbours and provide orientational information to a cell in a tissue (Lázaro-Diéguez and Müsch, 2017). In the epithelium, cell-cell adhesion is mediated by Adherens Junctions (AJs), with the principle component E-cadherin (E-cad), a transmembrane protein which binds in a homophilic fashion to E-cad molecules on adjacent cells (van Roy and Berx, 2008; Takeichi, 1977). Intracellularly E-cad interacts with the catenin protein family which consists of three members (Ozawa et al., 1990; Shapiro and Weis, 2009). At its distal C-terminus E-cad binds β-catenin, with α-catenin binding β-catenin and actin, thus tethering extracellular adhesion with the cytoskeleton. The third member, p120-catenin (p120ctn) binds to the JuxtaMembrane Domain (JMD) in the proximal C-terminus of E-cad (Davis et al., 2003).

The spatio-temporal expression and localization of E-cad is a prerequisite for the development of multi-cellular organisms: mutations of E-cad result in early embryonic lethality (Shimizu et al., 2005). The loss of E-cad from the cell surface has been implicated in the progression of cancer cells towards metastatic spread (Elisha et al., 2018). Concurrently, the return of E-cad to the plasma membrane is required for cells to re-integrate into tissues to form secondary tumours (Petrova et al., 2016; Wells et al., 2008). Therefore, knowledge of the mechanisms that modulate E-cad levels at the cell surface is crucial for understanding regulation of E-cad in development and disease.

E-cad has multiple levels of regulation, with endocytic recycling providing a rapid response to changing tissue tension or dynamics (Levayer et al., 2011; Troyanovsky et al., 2006). The catenin family member, p120ctn, is emerging as the key regulator of E-cad endocytosis and recycling (Bulgakova and Brown, 2016; Ireton et al., 2002; Sato et al., 2011). p120ctn was first described as a Src substrate in cancer cells (Reynolds et al., 1989)

and subsequently found to be a core component of the AJs (Thoreson et al., 2000). In mammalian cells, p120ctn is required to maintain E-cad at the plasma membrane: uncoupling p120ctn from E-cad or suppressing its expression results in complete internalization of E-cad (Davis et al., 2003; Ireton et al., 2002), which has been reported in several cancers (Gold et al., 1998; Shibata et al., 2004; van de Ven et al., 2015). Thus, a "Cap Model" was proposed whereby the binding of p120ctn to E-cad concealed endocytosis triggering motifs (Nanes et al., 2012; Reynolds, 2007). This model of unidirectional p120ctn activity has recently been challenged in mammalian cells, when it was found that p120ctn promotes endocytosis of E-cad through interaction with Numb (Sato et al., 2011). By contrast, in *Drosophila* and *C. elegans* p120ctn was thought less important because genetic ablation failed to replicate the effects observed in mammalian systems (Myster et al., 2003; Pacquelet et al., 2003; Pettitt et al., 2003). However, it has recently been reported that *Drosophila* p120ctn is required to stabilize E-cad in the pupal wing (Iyer et al., 2018) and promotes the endocytosis and recycling of E-cad in the embryo and larval wing discs (Bulgakova and Brown, 2016), indicating an evolutionary conservation of p120ctn function not previously appreciated.

One key aspect of endocytic regulation of cell adhesion is the remodelling of the actin cytoskeleton by small GTPases, particularity of the cortical actin which lies parallel to the plasma membrane (Baum and Georgiou, 2011; Cavey and Lecuit, 2009; Smythe and Ayscough, 2006) . One of the best characterised of these GTPase regulators is RhoA, whose activity results in focal points of actin contraction. The interaction between Rho and E-cad has been well documented in mammalian systems, and is important for cancer cell progression and anoikis resistance of tumours (Derksen and van de Ven, 2017). In *Drosophila*, Rho promotes the regulated endocytosis of E-cad by Dia and AP2 (Levayer et al., 2011). Conversely, Rho activity antagonises endocytic events in the early embryo (Lee and Harris, 2013), indicating the pivotal role RhoA plays in E-cad endocytic dynamics. The

evidence that p120ctn has a role in the RhoA pathway is contested, with evidence for and against, due to the different tissues and genetic tools used (Fox and Peifer, 2007; Fox et al., 2005; Magie et al., 2002).

Another group of GTPases important in the endocytosis of E-cad are Arf (ADP-Ribosylating Family) proteins (Paterson et al., 2003). Arf GTPases are members of the Ras superfamily and recruit coat proteins to facilitate the intracellular trafficking of vesicles. The first member of the family, Arf1, is classically viewed as a Golgi resident and responsible for anterograde transport from the Golgi to the plasma membrane (Donaldson and Jackson, 2011; McMahon and Boucrot, 2011). Recently, however, Arf1 was detected at the plasma membrane and participates in trafficking by co-operating with Arf6-dependent endocytosis (Humphreys et al., 2013; Padovani et al., 2014). Arf1 activity has been suggested to balance the initiation and impediment of endocytosis (Lee and Harris, 2013). In *Drosophila*, Arf1 is required for the remodelling of the actin cytoskeleton and facilitating endocytosis in the early syncytial embryo (Humphreys et al., 2012; Lee and Harris, 2013; Rodrigues et al., 2016). Furthermore, Arf1 interacts with E-cad and another component of AJs, Par-3 (Shao et al., 2010; Toret et al., 2014).

Here, we demonstrate that p120ctn acts to both inhibit and promote endocytosis of E-cad in a dynamic fashion within the same tissue. These activities are dependent on the amount of p120ctn at the plasma membrane and determine the levels and dynamic properties of E-cad. Further, we show that the interaction of p120ctn with Rho and Arf1 signalling pathways regulates clathrin-mediated endocytosis, with these two pathways acting in a hierarchical fashion to set the E-cad turnover rate. Additionally, we found that p120ctn determines tension at the tissue-level. Finally, we present a new model by which p120ctn fine-tunes adhesion through the regulation of actin dynamics, E-cad endocytosis, and thus modulates tissue tension.

Results

Both loss and overexpression of p120ctn stabilize E-cadherin at the plasma membrane via clathrin-mediated endocytosis

In previous work, where the requirement of p120ctn for E-cad endocytosis in *Drosophila* was discovered (Bulgakova and Brown, 2016), an E-cad expressed from a ubiquitous (*Ubi-p63E*) promoter was used (*Ubi::E-cad*-GFP). We first sought to substantiate previous findings using an E-cad tagged at its endogenous locus: *shotgun::*E-cad-GFP (hereafter, E-cad-GFP). The cells of the epidermis of stage 15 *Drosophila* embryos exhibit a distinct rectangular morphology (Fig. 1A) with long Anterior-Posterior (AP) axis cell borders and short Dorsal-Ventral (DV) axis cell borders. E-cad-GFP localized asymmetrically at this stage with a 1:2 (AP:DV) ratio between the two cell borders (Fig. 1A-C, Supplementary Table S1) (Bulgakova et al., 2013). In the absence of both maternal and zygotic p120ctn, the amount of E-cad was reduced at both the AP and DV cell borders by approximately 15% ($p=0.008$ and $p=0.035$, respectively, Fig. 1A-C).

Additionally, we measured the dynamics of E-cad-GFP using Fluorescence Recovery After Photobleaching (FRAP). In previous work, using the *Ubi::*E-cad-GFP, recovery of the signal intensity at the membrane was 70% for DV and 50% for the AP plasma membranes in control. Recovery curves were best-fit by a bi-exponential model (Bulgakova *et al*., 2013), with the fast and slow recovery components attributed to diffusion and endocytic recycling, respectively (Bulgakova et al., 2013; Iyer et al., 2018; Lippincott-Schwartz et al., 2003). The recovery was reduced to approximately 35% at both cell borders in *p120ctn* mutant embryos (Bulgakova and Brown, 2016). In the *p120ctn* mutant, a single exponential curve best described the data indicating that in the absence of p120ctn the slow recovery component observed in normal embryos was absent (Bulgakova and Brown, 2016). We replicated the above experiments using endogenously tagged E-cad-GFP, confirming that the effect of

p120ctn loss was the same when E-cad was expressed at endogenous levels (Supplementary Fig. S1, best-fit data in Supplementary Table S1). Combining our results with published data, we conclude that p120ctn loss leads to the stabilization of E-cad at the membrane by affecting the slow endocytic component of recovery (de Beco et al., 2009; Bulgakova and Brown, 2016; Bulgakova et al., 2013).

To further explore the function of p120ctn we examined the effect of overexpression on E-cad. In mammalian cell culture, overexpression of p120ctn results in the elevation of E-cad at plasma membranes by inhibiting endocytosis (van Hengel and van Roy, 2007), and recent studies indicate that p120ctn overexpression is implicated in the formation of secondary tumours by facilitating a mesenchymal-to-epithelial transition (Elisha et al., 2018; Goto et al., 2017). We created a p120ctn overexpression construct under the control of a *UAS* promoter (*UAS*::p120ctn). We expressed it in the posterior of each embryonic segment using the *engrailed*::GAL4 (*en*::GAL4) driver (Fig. 1D). This resulted in an increase of E-cad-GFP at AP but not DV cell borders relative to the adjacent internal control cells ($p=0.002$ and $p=0.27$, respectively, Fig. 1E, Table S1). The result at the AP border was the reverse of that observed for the *p120ctn* mutant (Fig. 1C, Supplementary Table S1). The absence of an increase at the DV might be due to E-cad being saturated at these borders in normal conditions. Measuring the dynamics of E-cad-GFP, using FRAP, we discovered that E-cad-GFP was less dynamic at both border types of the p120ctn overexpressing cells. Recovery was approximately 45% and 30% for AP and DV borders respectively (Fig. 1F). Additionally, the slow recovery phase was lost, comparable to that observed in the case of p120ctn loss, indicating impairment of endocytic recycling (best-fit data in Supplementary Table S1). The rate of fast recovery phase was the same in all cases. Therefore, both loss and overexpression of p120ctn impaired E-cad mobility and internalization.

Previously, the function of p120ctn in E-cad endocytosis was studied by measuring the localization and internalization rate of E-cad (Davis et al., 2003; Pieters et al., 2016). We decided to directly examine the effect p120ctn has on components of the endocytic machinery and determine if p120ctn acts through clathrin-mediated endocytosis. We used Clathrin Light Chain (CLC) tagged with GFP (*UAS*::CLC-GFP), to monitor clathrin localization and behaviour. CLC-GFP expressed using *en*::GAL4 was found in spots (puncta) co-localizing with the E-cad on the plasma membrane in the plane of AJs and to a lesser extent in the cytoplasm (Fig. 2A), a localization consistent with the known cellular function (Kaksonen and Roux, 2018). In the absence of p120ctn we observed a change in localization with more signal localizing with the E-cad at the membranes (Fig. 2B). Quantification of the puncta (see Materials and Methods) revealed that in the absence of p120ctn, CLC-GFP puncta were larger in area, fewer in number and more intense ($p=0.002$, $p=0.0001$, and $p=0.0003$, respectively, Fig. 2C-2E). Combining these measurements indicated that the overall CLC-GFP protein content was increased in the plane of the AJs in the p120ctn mutant ($p=0.0031$, Fig. 2F). To explore the effect of p120ctn on clathrin dynamics we measured CLC-GFP recovery in the plane of the AJs using FRAP and found that CLC-GFP in the *p120ctn* mutant embryos was substantially less mobile, indicated by a smaller mobile fraction ($p=0.0001$, Fig. 2G).

As E-cad had a smaller mobile fraction in p120ctn overexpression (Fig. 1H) we sought to determine whether this was due to an effect on the clathrin-mediated endocytic pathway. To explore this, we overexpressed p120ctn in conjunction with CLC-GFP. To balance the GAL4-UAS copy number, we co-expressed CD8-Cherry with CLC-GFP in the control (Fig 2H). CLC-GFP puncta in the p120ctn overexpressing cells were smaller in area and less intense ($p=0.01$ and $p=0.03$, respectively, Fig. 2I-2L), and overall protein content was unchanged (Fig. 2M), indicating a probable defect in the formation of mature vesicles

which abscise from the membrane. Finally, measuring the dynamics of CLC-GFP in these cells revealed that p120ctn overexpression reduced the mobile fraction of CLC-GFP ($p=0.0001$, Fig. 2N). Therefore, as both the removal and overexpression of p120ctn resulted in reduction of clathrin mobility, we reasoned that p120ctn levels act in a bell-curve fashion to regulate clathrin-mediated endocytosis of E-cad.

p120ctn acts via the Rho signalling pathway to stabilize E-cad at the adherens junctions

A primary candidate to link p120ctn to clathrin-mediated endocytosis is the GTPase RhoA. To ascertain whether p120ctn acts on clathrin-mediated endocytosis through regulating Rho signalling we turned to the downstream effectors of RhoA: the enzyme Rho-Kinase (Rok) and the actin cross-linker non-muscle Myosin II (Amano et al., 2010; Schwayer et al., 2016).

We used a tagged kinase-dead variant of Rok (Venus-Rok^{K116A}, hereafter referred to as Rok-Venus) driven by the *spaghetti squash* promoter to measure localization without overexpression (de Matos Simões et al., 2010). In the epidermis we observed a distinct asymmetry of Rok-Venus localisation between the AP and DV cell borders in the order 2:1 (AP:DV, Fig.3A-D) consistent with previous reports (Bulgakova et al., 2013; de Matos Simões et al., 2010). In the *p120ctn* mutant embryos we detected a loss of this asymmetry, specifically due to a reduction of the Rok-Venus levels at the AP cell borders ($p=0.013$, Fig. 3A-C). To confirm the interaction between p120ctn and Rok, we examined the effect of p120ctn overexpression. We found an increase in the amount of Rok-Venus at the AP cell borders ($p=0.0043$, Fig. 3A-B,D). Therefore, the levels of Rok-Venus at the plasma membrane mirror those of p120ctn.

To directly demonstrate an effect of p120ctn on the cytoskeleton we used an endogenously tagged variant of the non-muscle Myosin II (MyoII-YFP). The localization of the MyoII-YFP protein corresponded to that of Rok-Venus (Fig. 3E-F). The loss of p120ctn

resulted in the same effect on MyoII-YFP as that observed on Rok-Venus: loss of asymmetry due to a reduction at the AP cell borders (p=0.0011, Fig. 3E-G). Similarly, p120ctn overexpression resulted in an increase of MyoII-YFP at the AP plasma membrane by comparison to the internal control (p=0.025, Fig. 3E-F,H). Together, these results support a mechanism whereby p120ctn activates Rho signalling in a dose-dependent manner.

Having established an interaction between RhoA and p120ctn, we next examined the impact on E-cad endocytosis using constitutively active (Rho^{CA}) and dominant negative (Rho^{DN}) constructs to modulate Rho signalling. Dampening of Rho activity using suppression of the activator RhoGEF2 reduced E-cad levels at plasma membranes (Bulgakova et al., 2013). As this was a mild suppression by RNAi we decided to measure the effect of expressing Rho^{DN}. Expressed using the strong driver *en::GAL4*, it resulted in a complete loss of E-cad at the membrane by stage 15 of embryogenesis (data not shown). Therefore, we acutely induced the expression of the Rho^{DN} using temperature sensitive $GAL80^{ts}$ expressed from the *tubulin84B* promoter (Pilauri et al., 2005). We measured the amount of E-cad-GFP at the plasma membranes four hours post-induction of the Rho^{DN} expression, with time adjusted to obtain stage 15 of embryogenesis. In this case, cells presented the residual E-cad-GFP at the plasma membranes but, strikingly, it was reduced to discrete puncta along the membrane (arrowhead, Fig. 4A). The levels of E-cad-GFP at the plasma membranes were reduced at the AP cell borders (p=0.0039, Fig. 4B).

To complement these data, we examined the effect of overactivation of Rho signalling using the Rho^{CA} construct. This construct resulted in stark changes in cell morphology (Supplementary Fig. 2) and an increase of E-cad-GFP membrane levels at DV cell borders (p<0.0001, Fig. 4C-D). Due to cells rounding up (Supplementary Fig. 2), we also measured the mean intensity of E-cad-GFP at the membrane of these cells as a total of the entire membrane rather than dividing into AP and DV. As expected this analysis supported the

previous result: E-cad-GFP intensity was significantly increased in the Rho^{CA} cells ($p<0.0001$, Supplementary Fig. 2). Overall, these results showed that RhoA activity positively correlated with E-cad localization at the plasma membrane.

To investigate if the observed effects of manipulating Rho activity were the result of an endocytic mechanism, we measured the effects of these Rho constructs on clathrin using CLC-GFP. Co-expression of CLC-GFP with Rho^{CA} resulted in a localization change of the clathrin puncta in comparison to co-expression with CD8-Cherry in the control (Fig. 4E). A larger proportion of protein was localizing with E-cad at the membrane, and the puncta were of greater area and fewer in number ($p=0.0009$ and $p<0.0001$, respectively, Fig. 4F, 4H). Finally, we measured the dynamics of clathrin in these cells. The recovery of CLC-GFP was lower ($p<0.0001$, Fig. 4I), suggesting that the Rho activity impedes the formation of mature clathrin coated vesicles. In conclusion, our data is consistent with p120ctn-dependent activation of Rho signalling resulting in the inhibition of clathrin mediated endocytosis, enabling p120ctn to stabilize E-cad at the cell surface.

p120ctn promotes the internalization of E-cadherin through Arf1 signalling

Due to the reported interactions of Arf1 with E-cad and Par-3 (Shao et al., 2010; Toret et al., 2014) we decided to examine if Arf1 acts downstream of p120ctn. We used a transgenic GFP tagged variant of Arf1 (*UAS*::Arf1-GFP) driven by *en::*GAL4. Expressing this transgene in the epidermis we observed large and distinct puncta in the cytoplasm, corresponding to the Golgi (Supplementary Fig. S3), and to a lesser extent at the plasma membranes (Fig. 5A, highlighted by arrows). As we were interested in the activity of Arf1 at the plasma membrane not the Golgi we excluded the large puncta signal from our quantification (see Materials and Methods). Removing p120ctn resulted in a decrease in the amount of Arf1-GFP at the membrane, affecting both the AP and DV cell borders ($p<0.0001$ and $p<0.0001$, respectively,

Fig. 5A-C). In a complementary experiment, we overexpressed p120ctn: in these cells the amount of Arf1-GFP at the membrane was reduced at the AP border plasma membranes ($p=0.02$, Fig. 5D-F). Therefore, both the loss and overexpression of p120ctn reduced the amount of Arf1 at the membrane. This was highly reminiscent of the result we observed for clathrin. Moreover, as Arf1 is a known recruiter of clathrin at the Golgi, we inferred that plasma membrane Arf1 is downstream of p120ctn, which links it to clathrin-mediated endocytic machinery.

Having determined an interaction between p120ctn and Arf1, we next asked whether Arf1 activity had a more directive role in p120ctn mediated endocytosis of E-cad. Expression of a dominant negative variant of Arf1 ($Arf1^{DN}$, Wang et al., 2017) using the *en*::GAL4 driver increased the amount of E-cad-GFP at the plasma membrane at the AP borders with no change detected at the DV ($p=0.02$, Fig. 6A-B). This was accompanied by an abnormal cell morphology (Fig. 6A and Supplementary Fig. S4). No surviving larvae were observed, consistent with previous reports using $Arf1^{DN}$ in *Drosophila* (Carvajal-Gonzalez et al., 2015). We attributed this lethality to perturbation of post-Golgi protein transport by prolonged exposure to $Arf1^{DN}$, leading to cell death (Jian et al., 2010; Luchsinger et al., 2018).

To ascertain if Arf1 was acting on E-cad membrane localization via clathrin we measured the effect of expressing $Arf1^{DN}$ on the localization and amount of CLC-GFP. Co-expression of CLC-GFP with $Arf1^{DN}$ resulted in a substantial reduction in CLC-GFP puncta area, intensity, and number ($p<0.0001$, $p=0.0005$, and $p<0.0001$, respectively, Fig. 6C-F). Multiplying these values, we found an overall reduction in the amount of clathrin protein in the $Arf1^{DN}$ cells ($p<0.0001$, Fig. 6G). Therefore, Arf1 is required for the normal recruitment and function of clathrin at the AJs.

Finally, to confirm that Arf1 is functionally downstream of p120ctn we designed a rescue experiment using a constitutively active Arf1 ($Arf1^{CA}$). We expressed this in a *p120ctn*

mutant background and measured the effect on CLC-GFP (see Fig. 2). We compared this to control co-expressing CLC-GFP with CD8-Cherry in an otherwise wild-type genetic background. Control clathrin puncta localization was as previously observed (Fig. 6H). In the *p120ctn* mutant expressing $Arf1^{CA}$ the clathrin puncta were no different in area, intensity or number from control (p=0.21, p=0.19, and p=0.33, respectively, Fig, 6I-L). Measuring the dynamics of clathrin revealed that recovery was no longer significantly different from the wild-type control (Fig. 6M). From both fixed and dynamic measures of clathrin we concluded that the expression of $Arf1^{CA}$ rescues the clathrin defect observed in the *p120ctn* mutant (see Fig. 2). Therefore, Arf1 functionality is consistent with it being a downstream interactor of p120ctn, which links the p120ctn–E-cad complex to the clathrin-mediated endocytic machinery. Overall, this allows p120ctn to promote the internalization of E-cad in addition to the previously described anti-endocytic function.

The Rho signalling pathway is upstream of Arf1

Having established that Arf1 and RhoA signalling are regulated by p120ctn, resulting in the internalization or retention of E-cad respectively, we sought to determine if these two pathways act upon one another or exist independently. To address this, we perturbed signalling in one pathway and measured the effect on the other.

First, we measured the membrane localization of MyoII-YFP, as a readout of RhoA signalling activity, upon upregulation of Arf1 signalling using $Arf1^{CA}$. MyoII-YFP localization was indistinguishable between cells expressing $Arf1^{CA}$ and control cells (Fig. 7A-B), demonstrating that Rho signalling is independent of Arf1 function. In a complementary experiment, we impaired RhoA signalling using an RNAi against the upstream activator RhoGEF2, which results in a milder E-cad reduction at AJs than the severe loss observed with Rho^{DN} expression (Fig. 4 and Bulgakova et al., 2013). We

measured the membrane levels of Arf1-GFP in cells additionally expressing either RhoGEF2-RNAi or CD8-Cherry (Fig. 7C, D). Downregulation of RhoGEF2 resulted in a significant increase in the amount of Arf1-GFP at both AP and DV borders ($p=0.045$ and $p=0.022$, respectively, Fig. 7E), demonstrating that RhoA inhibits Arf1 localization to the plasma membrane. This was reminiscent of the phenotype observed upon p120ctn overexpression, in which Arf1 is reduced at the plasma membrane (see Fig. 5). Therefore, as the overexpression of p120ctn is accompanied by upregulation of Rho signalling (see Fig. 3), we suggest that the reduction of Arf1 previously observed (Fig. 5) is caused by the regulation of Arf1 recruitment by Rho signalling. However, the reduction of Arf1 at the plasma membrane in the absence of p120ctn (see Fig. 5) is independent of RhoA and is caused by regulation of Arf1 recruitment and/or activation more directly by p120ctn.

p120ctn levels modulate plasma membrane tension

Having identified two actin-remodelling pathways downstream of p120ctn we sought to understand their functional outcome at the tissue-level. Actin assembly on clathrin-coated pits, which requires Arf activity (Myers and Casanova, 2008), is suggested to counteract cortical tension to enable membrane deformation (Boulant et al., 2011). In light of the MyoII results, we decided to test if p120ctn modulated membrane tension. We analysed this using microablation of membranes and measured the initial recoil as a readout of tissue tension (Mao et al., 2013). We examined AP membranes as these presented an enrichment of MyoII (see Fig. 3). The initial recoil is proportionally influenced by the underlying tension in the system rather than other variables (Liang et al., 2016), thus we decided to focus our attention on this measure. The initial recoil was measured as the distance between the two connected cell vertices of the ablated membrane immediately post-ablation, expressed as a change in the length proportional to pre-ablation length (Fig. 8A). In control embryos expressing E-cad-

GFP alone, the recoil distance post-ablation showed an increase of 5% over pre-ablation distance (Fig. 8A-B). The overexpression of p120ctn resulted in a higher mean initial recoil of 10% over the pre-ablation distance ($p<0.0001$, Fig 8A-B). Conversely, in *p120ctn* mutant cells the recoil was decreased ($p=0.022$) to a mean value of 2% increase over pre-ablation distance (Fig. 8A-B). Therefore, membrane tension positively correlated with p120ctn.

Discussion

In this study we have focused on the mediators and mechanism of E-cad turnover downstream of p120ctn. We present several advances to the understanding of p120ctn activity and its role in cell-cell adhesion. First, we showed that p120ctn acts bi-directionally as a set point for E-cad at the plasma membrane via a clathrin-mediated mechanism. Second, we demonstrated that p120ctn activates RhoA signalling, which regulates the internalization of E-cad. This places *Drosophila* p120ctn in the same context as its mammalian orthologue, which interacts with Rho depending upon p120ctn sub-cellular localization (van Hengel and van Roy, 2007). Third, we discovered an Arf1 dependent mechanism by which p120ctn promotes the internalization of E-cad. Finally, we have collated our results into a new model of p120ctn action. This describes the activity of p120ctn as a function of the differential interaction with RhoA and Arf1 (Fig. 8C). In this model, p120ctn regulates membrane tension through RhoA, reinforcing cortical actin, which inhibits E-cad endocytosis. Simultaneously, p120ctn regulates the formation of clathrin-coated vesicles through Arf1, promoting E-cad endocytosis, until a threshold is passed and further increase of p120ctn results in Arf1 inhibition, due to the concordant increase in RhoA activity. Altogether, the balance between these pathways depends on p120ctn levels and determines the amount of E-cad endocytosis. Therefore, we suggest that p120ctn provides a central hub to co-ordinate cell

adhesion with endocytosis and the actin cytoskeleton to dictate cellular behaviour and tissue tension.

Previous work established a cap model whereby p120ctn only prevents the internalization of E-cad (van Hengel and van Roy, 2007). This function is ascribed to two motifs in mammalian E-cad (LL and DEE), which are absent in *Drosophila* E-cad (Nanes et al., 2012). This explains why *Drosophila* E-cad is not completely internalised in *p120ctn* mutants (Myster et al., 2003). Here, we showed that p120ctn overexpression inhibits E-cad endocytosis. Superficially, this is similar to mammalian cells, in which stabilization results from p120ctn outcompeting access to the E-cad DD and DEE motifs. However, our findings represent a distinct phenomenon resulting from the perturbed balance of downstream signalling.

Both Rho and Arf1 regulate actin remodelling and endocytosis, but their functions are fundamentally different. RhoA has been one of the most well studied elements of the regulated remodelling of the actin cytoskeleton (Hodge and Ridley, 2016). Its distribution and recruitment of various components lead to increasing cortical tension via the phosphorylation of non-muscle Myosin II. In turn, increased cortical tension counteracts membrane bending which is required for vesicle formation and endocytosis (Curtis and Meldolesi, 2012; Jarsch et al., 2016). Prior to our work a debate existed about p120ctn acting via RhoA signalling in *Drosophila* (Fox et al., 2005; Magie et al., 2002), we have resolved this by evidencing that Rho activity correlates with p120ctn levels at the membrane. Further we have shown that the functional outcome of this p120ctn-Rho interaction is to stabilize E-cad. Elevated p120ctn and RhoA activity impairs the formation of vesicles to internalize E-cad, and therefore increases the duration E-cad spends at the membrane, shifting the set point of steady-state E-cad membrane levels.

In contrast, Arf1 promotes E-cad endocytosis by both recruiting clathrin adaptor proteins and facilitating the remodelling of actin required for vesicle formation and abscission. In this study we showed for the first time a role for Arf1 in the clathrin-mediated trafficking of E-cad from the membrane. Prior to our work the Arf1 recruitment of clathrin had only been shown to occur at the Golgi by recruiting the Adaptor 1 protein (AP1) (Carvajal-Gonzalez et al., 2015). The function of Arf1 at the plasma membrane had been descried in dynamin-independent endocytosis, which was presumed to be clathrin-independent (Kumari and Mayor, 2008). However, the involvement of Arf1 in multiple endocytic pathways has not been fully explored. We have shown that Arf1's capacity to recruit clathrin is exploited by p120ctn to facilitate the endocytosis of E-cad. Whether this requires AP2, a well-documented membrane resident clathrin adaptor, has yet to be determined. Our findings provide a mechanistic insight into the pro-endocytic activity of p120ctn which has only recently come to light (Bulgakova and Brown, 2016; Sato et al., 2011) and elaborates the limited number of known p120ctn interactors. The activities of Arf1 and RhoA are antagonistic, which was also seen in previous studies on the cellularization of the early embryo (Lee and Harris, 2013). In light of our findings, we propose they act in a hierarchical fashion with RhoA predominating over Arf1, presumably indirectly by increasing the density of cortical actin. We propose that by balancing these two pathways p120ctn determines the precise amount of E-cad endocytosis. Further, using laser ablation we demonstrated that p120ctn directly modulates tension, providing a broader view for the function of p120ctn on the tissue-level. Considering that all of the components of this non-linear regulatory network are expressed in all epithelia across evolution, we speculate that this system is likely to be more broadly applicable in development and a general feature of cell biology.

Members of the p120ctn family are highly evolutionarily conserved, with primordial armadillo domain proteins present in single cell organisms without cell-cell adhesion, implying a function which predates the evolution of cell adhesion molecules (Carnahan et al., 2010; Gul et al., 2017). Later work ascribed this to the conserved function of all catenins in the regulation or remodelling of actin, which is present even in unicellular organisms (Abedin and King, 2010). Thus, it appears that during the course of evolution the machinery, which evolved to modulate the actin cytoskeleton, was co-opted by cell adhesion molecules to link extracellular attachment to the internal cytoskeleton. Our work supports this view by showing that p120ctn acts on E-cad endocytosis through the regulation of two actin remodelling machineries: Arf1 and Rho signalling. It is probable that the mechanisms we have discovered are conserved in higher organisms. We speculate that this has been further elaborated in mammalian cells, evidenced by the multiplication of the p120ctn family, each of which has several isoforms (Pieters et al., 2012). This is necessitated by the increased complexity and variety of mammalian tissues and by the longevity of mammalian organisms.

We conclude that p120ctn acts in a dose-dependent manner on Rho and Arf1 signalling, indicating that the levels of p120ctn are a set point for E-cad turnover. An important question for future work will be to examine the extent to which the mechanisms we have described in this work are conserved in higher organisms and to define what effect this has upon development and disease.

Materials and Methods

Fly stocks and genetics

Flies were raised on standard medium. The GAL4/UAS system (Brand and Perrimon, 1993) was used for all the specific spatial and temporal expression of transgenic and RNAi experiments. The GAL4 expressional driver used for all experiments was *engrailed::GAL4* (*en*::GAL4, Bloomington number 30564). The following fly stocks were used in this study (Bloomington number included where applicable): E-cad-GFP (*shg::E-cadherin-GFP*) (60584), Shg-Cherry (*shg::mCherry*, 59014), *UAS*::CLC-GFP (7109), *UAS*::Arf1-GFP (gift from T.Harris), Zipper-YFP (*Myosin II*-YFP, Kyoto Stock Center 115082), *sqh*::Rok^{K116A}-Venus (gift from J.Zallen), *UAS*::Arf1-T31N (DN) and *UAS::*Arf1-Q71L (CA) (Wang et al., 2017), *UAS*::Rho1-N19 (DN) (7328), and *tubulin*::GAL80^{TS} (7017). The p120ctn mutant genotype (p120ctn^{308}/ Δp120) used was derived from crossing two deficiency stocks: homozygously viable p120ctn^{308} females (Myster et al., 2003) with homozygously lethal Df(2R)M41A8/ CyO, *twi::*Gal4, *UAS::*GFP males (740). Thus, the p120ctn mutants examined lacked both maternal and zygotic contributions.

Embryo collection and fixation

Embryos were collected at 25°C at 3-hour time intervals and allowed to develop at 18°C for 21 hours to reach the desired developmental stage, except for the acute induction experiments, where embryos were allowed to develop for 13 hours at 18°C and shifted to 29°C for 4 hours. Then embryos were dechorionated using 50% sodium hypochlorite (bleach, Invitrogen) in water for 4 minutes, and extensively washed with deionized water prior to fixation. Fixation was performed with a 1:1 solution of 4% formaldehyde (Sigma) in PBS (Phosphate Buffered Saline) and heptane (Sigma) for 20 minutes on an orbital shaker at room temperature. Embryos were then devitellinized in 1:1 solution of methanol and heptane for 20

sec with vigorous agitation. Following subsequent methanol washes the fixed embryo specimens were stored at -20°C in methanol until required.

Embryo live imaging

Embryos were collected and dechorionated as described above. Once washed with deionized water embryos were transferred to apple juice agar segments upon microscope slide. Correct genotypes were selected under a fluorescent microscope (Leica) using a needle. Embryos were positioned and orientated in a row consisting of 6-10 embryos per genotype. Following this, embryos were transferred to pre-prepared microscope slides with Scotch tape and embedded in Halocarbon oil 27 (Sigma). Embryos were left to aerate for 10 minutes prior to covering with a cover slip and imaging.

For laser ablation, following orientation and positioning the embryos were transferred to a 60mm x 22mm coverslip which had been pre-prepared by applying 10 µl of Heptane glue along a strip in the middle of the coverslip orientated with the long axis. The coverslip was attached to a metal slide cassette (Zeiss), and the embryos were embedded in Halocarbon oil 27 before imaging.

Molecular cloning

The p120ctn full length cDNA was obtained from Berkeley Drosophila Genome Project (BDGP), supplied in a pBSSK vector. This was sub-cloned into a (pUAS-k10.attB) plasmid using standard restriction digestion with NotI and BamHI (New England Biolabs) followed by ligation with T4 DNA ligase (New England Biolabs) and transformation into DH5a competent E.coli cells (Thermo Fisher Scientific). Prior to injection plasmids were test digested and sequenced (Core Genomic Facility, University of Sheffield). Plasmids were prepared for injection using standard miniprep extraction (Qiagen) and submitted for

injection (Microinjection service, Department of Genetics, University of Cambridge) into the attP-86Fb stock (Bloomington stock 24749). Successful incorporation of the transgene was determined by screening for (w^+) in the F1 progeny.

Immunostaining

The embryos were washed three times in 1 ml of PBST (PBS with 0.05% Triton) with gentle rocking. Blocking of the embryos prior to staining was done in 300 µl of a 1% NGS (Normal Goat Serum) in PBST for 1 hour at room temperature with gentle rocking. For staining the blocking solution was removed, 300 µl of the primary antibody: either 1:100 dilution of a rat anti-E-cad (DCAD2, DSHB) or 1:10 of a mouse anti-engrailed (4D9, DSHB) in fresh blocking solution was added and the embryos were incubated overnight at 4°C with orbital rotation. Then, embryos were washed three times with 1 ml of PBST. A 300 µl 1:300 dilution of the secondary antibody (goat Cy3- or Cy5-conjugated anti-rat-IgG, Invitrogen) was added, and the embryos incubated either overnight at 4°C with orbital rotation or for 2 hours at room temperature with gentle rocking. Then embryos were washed three time with PBST, following which they were incubated with 50-70 µl of Vectashield (Vector Laboratories) and allowed to equilibrate for a period of 2 hours before being mounted on microscope slides (Thermo).

Microscopy, data acquisition and FRAP

All experiments except for laser ablation were performed using an up-right Olympus FV1000 confocal microscope with a 60x/1.40 NA oil immersion objective. All measurements were made on dorsolateral epidermal cells of embryos, which were near or just after completion of dorsal closure, corresponding to the end of Stage 15 of embryogenesis. For fixed samples 16-bit images were taken at a magnification of 0.051µm/pixel (1024x1024 pixel XY-image) with

a pixel dwell of 4µm/pixel. For each embryo, a Z-axis sectional stack through the plane of the AJs was taken, which consisted of six sections with a 0.38 µm intersectional spacing. The images were saved in the Olympus binary image format for further processing.

For E-cad FRAP (adapted from Bulgakova et al., 2013) 16-bit images were taken at a magnification of 0.093 µm/pixel (320x320 pixel XY-image). In each embryo, several circular regions of 1 µm radius were photobleached at either DV or AP junctions resulting in one bleach event per cell. Photobleaching was performed with 8 scans at 2 µs/pixel at 50-70% 488 nm laser power, resulting in the reduction of E-cad-GFP signal by 60–80%. A stack of 6 z-sections spaced by 0.38 µm was imaged just before photobleaching, and immediately after photobleaching, and then at 20 s intervals, for a total of 15 minutes.

For CLC-GFP FRAP, 16-bit images were taken at a magnification of 0.051µm/pixel (256x256 pixel XY-image). In each embryo a single plane was selected in centre of the AJ band using Shg-Cherry for positioning. An area encompassing a transverse region orthogonal to the axis of the engrailed expressing cells was selected (140x60 pixels) was photobleached with 1 scan at 2 µm/pixel using 100% 488nm laser power resulting in reduction of CLC-GFP signal by 70-80%. Images were taken using continuous acquisition at a frame rate of 2 sec^{-1}. Prior to bleaching a sequence of 10 images was taken, and a total of 400 frames corresponding to 3.5 minutes were taken.

Data processing and statistical analysis

Membrane intensity: Images were processed in Fiji (https://fiji.sc) by generating average intensity projections of the channel required for quantification. Masks were created by processing background-subtracted maximum intensity projections using the Tissue Analyzer plugin in Fiji (Aigouy and Bivic, 2016). Quantification of the membrane intensity at the AP and DV borders was done as described previously using a custom-built Matlab script

(Bulgakova and Brown, 2016) found at (https://github.com/nbul/Intensity). Statistical analysis was performed in Graphpad Prism (https://www.graphpad.com/scientific-software/prism/). First, the data was cleaned using ROUT detection of outliers in Prism followed by testing for normal distribution (D'Agostino & Pearson normality test). Then, the significance for parametric data was tested by either a two-way ANOVA or two-tailed t-test with Welch's correction.

E-cad FRAP: images were processed by using the grouped Z-projector plugin in Fiji to generate average intensity projections for each time-point. Following this the bleached ROI, control ROI and background intensity were manual measured for each time point. This data was processed in Microsoft Excel. First the intensity of the bleached ROI at each time point was background subtracted and normalized as following: $I_n = (F_n - BG_n)/(FC_n - BG_n)$, where F_n – intensity of the bleached ROI at the time point n, FC_n – intensity of the control unbleached ROI of the same size at the plasma membrane at the time point n, and BG_n – background intensity, measured with the same size ROI in cytoplasm at the time point n. Than the relative recovery at each time point was calculated using the following formula: $R_n = (I_n - I_1)/(I_0 - I_1)$, where I_n, I_1 and I_0 are normalized intensities of bleached ROI and time point n, immediately after photobleaching, and before photobleaching respectively. These values were input to Prism and nonlinear regression analysis was performed to test for best fit model and if recoveries were significantly different between cell borders or genotypes. The recovery was fit to either single exponential model in a form of $f(t) = 1 - F_{im} - A_1 e^{-t/T_{fast}}$, or to bi-exponential model in a form of $f(t) = 1 - F_{im} - A_1 e^{-t/T_{fast}} - A_2 e^{-t/T_{slow}}$, where F_{im} is a size of the immobile fraction, T_{fast} and T_{slow} are the half times, and A_1 and A_2 are amplitudes of the fast and slow components of the recovery. An F-test was used to choose the model and compare datasets.

CLC-GFP FRAP: measurements of all intensities, i.e. the bleached ROI, control ROI and the background, and normalization were done using a custom-build Matlab script (http://github.com/nbul/FRAP) using the same algorithm as described for E-cad FRAP. Curve fitting and statistical analysis was performed in Graphpad Prism using a nonlinear regression analysis as described for E-cad FRAP.

CLC-GFP puncta: Images were analysed using a custom script in MATLAB described in (Strutt et al., 2016). This was modified for unpaired data by calculating a threshold value for puncta detection using a mean calculated from all of the control images and applying this threshold to the experimental images. Statistical analysis of the recovery was performed in Graphpad Prism using nonlinear regression analysis.

Total membrane intensity: the masks generated using the Tissue analyser plugin were processed using a custom-built Matlab script (https://github.com/nbul/Intensity/tree/master/TissueAnalyzer). In short, the outlines of the cells were determined from the binary masks, and the length of outline was used as a measure of cell perimeter. Then, the outlines of individual cells were dilated using a YxY structuring element, so that the resulting mask covered all visible E-cad signal on the borders of the cell, and the mean pixel intensity of the mask was measured. The total protein amount was calculated as a product of cell perimeter by mean pixel intensity of the mask. Statistical analysis was performed in Graphpad Prism: using a two-tailed t-test with Welch's correction.

Laser Ablation

Nanoablation of single junctions was performed to provide a measure of junctional tension. Embryos were imaged on a Zeiss LSM 880 microscope with an Airyscan detector, an 8-bit image at 0.053 µm/pixel (512x512 pixel XY-Image) resolution with a 63x objective (NA 1.4) at 5x zoom and 2x averaging was used. An illumination wavelength of 488 nm and 0.5%

laser power were used. Images were captured with a 0.5 µm z-spacing. Narrow rectangular ROIs were drawn across the centre of single junctions and this region was ablated using a pulsed TiSa laser (Chameleon), tuned to 760 nm at 45% power. Embryos were imaged continuously in a z-stack consisting of 3 z-slices. The initial recoil rate of vertices at the ends of ablated junctions was quantified by measuring the change in distance between the vertices and dividing by the initial time step. Statistical analysis was performed in Graphpad Prism: using a two-tailed t-test with Welch's correction.

Acknowledgments

The authors first wish to thank Rob Tetley and Yanlan Mao for assistance with laser ablation experiments. The authors also with to acknowledge the advice and guidance of Professor David Strutt, University of Sheffield, and his lab. The authors thank to the technical staff of the Wolfson Light Microscopy Facility (LMF) and the Fly Facility, the University of Sheffield, without whom this work would not be possible. This work was supported by grant BB/P007503/1 from the UK Biotechnology and Biological Sciences Research Council.

Author Contribution

J.G and N.B. designed and performed experiments and wrote the manuscript.

Conflicts of Interest

The authors declare and confirm that there is no conflict of interest for the work presented in this paper.

Supplementary material

Supplementary data includes: a table containing all numerical values and statistics for the data presented in this work; the FRAP data for the endogenously tagged E-cad, which reproduces the results of the *Ubi::*E-cad (Fig 1); the cell morphology measurement of the Rho^{CA} expressing cells (Fig. 4); the immunostaining of Arf1-GFP to confirm cytoplasmic puncta localization to Golgi (Fig. 5); and cell morphology measurement of the $Arf1^{DN}$ expressing cells (Fig. 6)

References

Abedin, M., and King, N. (2010). Diverse evolutionary paths to cell adhesion. Trends Cell Biol. *20*, 734–742.

Aigouy, B., and Bivic, A.L. (2016). The PCP pathway regulates Baz planar distribution in epithelial cells. Sci. Rep. *6*, srep33420.

Amano, M., Nakayama, M., and Kaibuchi, K. (2010). Rho-Kinase/ROCK: A Key Regulator of the Cytoskeleton and Cell Polarity. Cytoskelet. Hoboken Nj *67*, 545–554.

Baum, B., and Georgiou, M. (2011). Dynamics of adherens junctions in epithelial establishment, maintenance, and remodeling. J. Cell Biol. *192*, 907–917.

de Beco, S., Gueudry, C., Amblard, F., and Coscoy, S. (2009). Endocytosis is required for E-cadherin redistribution at mature adherens junctions. Proc. Natl. Acad. Sci. U. S. A. *106*, 7010–7015.

Boulant, S., Kural, C., Zeeh, J.-C., Ubelmann, F., and Kirchhausen, T. (2011). Actin dynamics counteract membrane tension during clathrin-mediated endocytosis. Nat. Cell Biol. *13*, 1124–1131.

Brand, A.H., and Perrimon, N. (1993). Targeted gene expression as a means of altering cell fates and generating dominant phenotypes. Dev. Camb. Engl. *118*, 401–415.

Bulgakova, N.A., and Brown, N.H. (2016). Drosophila p120-catenin is crucial for endocytosis of the dynamic E-cadherin-Bazooka complex. J. Cell Sci. *129*, 477–482.

Bulgakova, N.A., Grigoriev, I., Yap, A.S., Akhmanova, A., and Brown, N.H. (2013). Dynamic microtubules produce an asymmetric E-cadherin–Bazooka complex to maintain segment boundaries. J. Cell Biol. *201*, 887–901.

Carnahan, R.H., Rokas, A., Gaucher, E.A., and Reynolds, A.B. (2010). The Molecular Evolution of the p120-Catenin Subfamily and Its Functional Associations. PLOS ONE *5*, e15747.

Carvajal-Gonzalez, J.M., Balmer, S., Mendoza, M., Dussert, A., Collu, G., Roman, A.-C., Weber, U., Ciruna, B., and Mlodzik, M. (2015). The clathrin adaptor AP-1 complex and Arf1 regulate planar cell polarity in vivo. Nat. Commun. *6*, 6751.

Cavey, M., and Lecuit, T. (2009). Molecular Bases of Cell–Cell Junctions Stability and Dynamics. Cold Spring Harb. Perspect. Biol. *1*.

Curtis, I. de, and Meldolesi, J. (2012). Cell surface dynamics – how Rho GTPases orchestrate the interplay between the plasma membrane and the cortical cytoskeleton. J Cell Sci *125*, 4435–4444.

Davis, M.A., Ireton, R.C., and Reynolds, A.B. (2003). A core function for p120-catenin in cadherin turnover. J Cell Biol *163*, 525–534.

Derksen, P.W.B., and van de Ven, R.A.H. (2017). Shared mechanisms regulate spatiotemporal RhoA-dependent actomyosin contractility during adhesion and cell division. Small GTPases 1–9.

Donaldson, J.G., and Jackson, C.L. (2011). ARF family G proteins and their regulators: roles in membrane transport, development and disease. Nat. Rev. Mol. Cell Biol. *12*, 362–375.

Elisha, Y., Kalchenko, V., Kuznetsov, Y., and Geiger, B. (2018). Dual role of E-cadherin in the regulation of invasive collective migration of mammary carcinoma cells. Sci. Rep. *8*, 4986.

Fox, D.T., and Peifer, M. (2007). Cell Adhesion: Separation of p120's Powers? Curr. Biol. *17*, R24–R27.

Fox, D.T., Homem, C.C.F., Myster, S.H., Wang, F., Bain, E.E., and Peifer, M. (2005). Rho1 regulates Drosophila adherens junctions independently of p120ctn. Development *132*, 4819–4831.

Gold, J.S., Reynolds, A.B., and Rimm, D.L. (1998). Loss of p120ctn in human colorectal cancer predicts metastasis and poor survival. Cancer Lett. *132*, 193–201.

Goto, W., Kashiwagi, S., Asano, Y., Takada, K., Takahashi, K., Hatano, T., Takashima, T., Tomita, S., Motomura, H., Ohsawa, M., et al. (2017). Circulating tumor cell clusters-associated gene plakoglobin is a significant prognostic predictor in patients with breast cancer. Biomark. Res. *5*.

Gul, I.S., Hulpiau, P., Saeys, Y., and van Roy, F. (2017). Evolution and diversity of cadherins and catenins. Exp. Cell Res. *358*, 3–9.

van Hengel, J., and van Roy, F. (2007). Diverse functions of p120ctn in tumors. Biochim. Biophys. Acta BBA - Mol. Cell Res. *1773*, 78–88.

Hodge, R.G., and Ridley, A.J. (2016). Regulating Rho GTPases and their regulators. Nat. Rev. Mol. Cell Biol. *17*, 496–510.

Humphreys, D., Liu, T., Davidson, A.C., Hume, P.J., and Koronakis, V. (2012). The Drosophila Arf1 homologue Arf79F is essential for lamellipodium formation. J. Cell Sci. *125*, 5630–5635.

Humphreys, D., Davidson, A.C., Hume, P.J., Makin, L.E., and Koronakis, V. (2013). Arf6 coordinates actin assembly through the WAVE complex, a mechanism usurped by Salmonella to invade host cells. Proc. Natl. Acad. Sci. *110*, 16880–16885.

Ireton, R.C., Davis, M.A., van Hengel, J., Mariner, D.J., Barnes, K., Thoreson, M.A., Anastasiadis, P.Z., Matrisian, L., Bundy, L.M., Sealy, L., et al. (2002). A novel role for p120 catenin in E-cadherin function. J. Cell Biol. *159*, 465–476.

Iyer, K.V., Piscitello-Gómez, R., Jülicher, F., and Eaton, S. (2018). Mechanosensitive binding of p120-Catenin at cell junctions regulates E-Cadherin turnover and epithelial viscoelasticity. BioRxiv 357186.

Jarsch, I.K., Daste, F., and Gallop, J.L. (2016). Membrane curvature in cell biology: An integration of molecular mechanisms. J Cell Biol *214*, 375–387.

Jian, X., Cavenagh, M., Gruschus, J.M., Randazzo, P.A., and Kahn, R.A. (2010). Modifications to the C-terminus of Arf1 alter cell functions and protein interactions. Traffic Cph. Den. *11*, 732–742.

Kaksonen, M., and Roux, A. (2018). Mechanisms of clathrin-mediated endocytosis. Nat. Rev. Mol. Cell Biol. *19*, 313–326.

Kumari, S., and Mayor, S. (2008). ARF1 is directly involved in dynamin-independent endocytosis. Nat. Cell Biol. *10*, 30–41.

Lázaro-Diéguez, F., and Müsch, A. (2017). Cell–cell adhesion accounts for the different orientation of columnar and hepatocytic cell divisions. J Cell Biol jcb.201608065.

Lee, D.M., and Harris, T.J.C. (2013). An Arf-GEF Regulates Antagonism between Endocytosis and the Cytoskeleton for Drosophila Blastoderm Development. Curr. Biol. *23*, 2110–2120.

Levayer, R., Pelissier-Monier, A., and Lecuit, T. (2011). Spatial regulation of Dia and Myosin-II by RhoGEF2 controls initiation of E-cadherin endocytosis during epithelial morphogenesis. Nat. Cell Biol. *13*, 529–540.

Liang, X., Michael, M., and Gomez, G.A. (2016). Measurement of Mechanical Tension at Cell-cell Junctions Using Two-photon Laser Ablation. Bio-Protoc. *6*.

Lippincott-Schwartz, J., Altan-Bonnet, N., and Patterson, G.H. (2003). Photobleaching and photoactivation: following protein dynamics in living cells. Nat. Cell Biol. *Suppl*, S7-14.

Luchsinger, C., Aguilar, M., Burgos, P.V., Ehrenfeld, P., and Mardones, G.A. (2018). Functional disruption of the Golgi apparatus protein ARF1 sensitizes MDA-MB-231 breast cancer cells to the antitumor drugs Actinomycin D and Vinblastine through ERK and AKT signaling. PloS One *13*, e0195401.

Magie, C.R., Pinto-Santini, D., and Parkhurst, S.M. (2002). Rho1 interacts with p120ctn and α-catenin, and regulates cadherin-based adherens junction components in Drosophila. Development *129*, 3771–3782.

Mao, Y., Tournier, A.L., Hoppe, A., Kester, L., Thompson, B.J., and Tapon, N. (2013). Differential proliferation rates generate patterns of mechanical tension that orient tissue growth. EMBO J. *32*, 2790–2803.

de Matos Simões, S., Blankenship, J.T., Weitz, O., Farrell, D.L., Tamada, M., Fernandez-Gonzalez, R., and Zallen, J.A. (2010). Rho-kinase directs Bazooka/Par-3 planar polarity during Drosophila axis elongation. Dev. Cell *19*, 377–388.

McMahon, H.T., and Boucrot, E. (2011). Molecular mechanism and physiological functions of clathrin-mediated endocytosis. Nat. Rev. Mol. Cell Biol. *12*, 517–533.

Myers, K.R., and Casanova, J.E. (2008). Regulation of actin cytoskeleton dynamics by Arf-family GTPases. Trends Cell Biol. *18*, 184–192.

Myster, S.H., Cavallo, R., Anderson, C.T., Fox, D.T., and Peifer, M. (2003). Drosophila p120catenin plays a supporting role in cell adhesion but is not an essential adherens junction component. J Cell Biol *160*, 433–449.

Nanes, B.A., Chiasson-MacKenzie, C., Lowery, A.M., Ishiyama, N., Faundez, V., Ikura, M., Vincent, P.A., and Kowalczyk, A.P. (2012). p120-catenin binding masks an endocytic signal conserved in classical cadherins. J Cell Biol *199*, 365–380.

Ozawa, M., Ringwald, M., and Kemler, R. (1990). Uvomorulin-catenin complex formation is regulated by a specific domain in the cytoplasmic region of the cell adhesion molecule. Proc. Natl. Acad. Sci. U. S. A. *87*, 4246–4250.

Pacquelet, A., Lin, L., and Rorth, P. (2003). Binding site for p120/delta-catenin is not required for Drosophila E-cadherin function in vivo. J. Cell Biol. *160*, 313–319.

Padovani, D., Folly-Klan, M., Labarde, A., Boulakirba, S., Campanacci, V., Franco, M., Zeghouf, M., and Cherfils, J. (2014). EFA6 controls Arf1 and Arf6 activation through a negative feedback loop. Proc. Natl. Acad. Sci. U. S. A. *111*, 12378–12383.

Paterson, A.D., Parton, R.G., Ferguson, C., Stow, J.L., and Yap, A.S. (2003). Characterization of E-cadherin Endocytosis in Isolated MCF-7 and Chinese Hamster Ovary Cells THE INITIAL FATE OF UNBOUND E-CADHERIN. J. Biol. Chem. *278*, 21050–21057.

Petrova, Y.I., Schecterson, L., and Gumbiner, B.M. (2016). Roles for E-cadherin cell surface regulation in cancer. Mol. Biol. Cell *27*, 3233–3244.

Pettitt, J., Cox, E.A., Broadbent, I.D., Flett, A., and Hardin, J. (2003). The Caenorhabditis elegans p120 catenin homologue, JAC-1, modulates cadherin-catenin function during epidermal morphogenesis. J. Cell Biol. *162*, 15–22.

Pieters, T., van Roy, F., and van Hengel, J. (2012). Functions of p120ctn isoforms in cell-cell adhesion and intracellular signaling. Front. Biosci. Landmark Ed. *17*, 1669–1694.

Pieters, T., Goossens, S., Haenebalcke, L., Andries, V., Stryjewska, A., De Rycke, R., Lemeire, K., Hochepied, T., Huylebroeck, D., Berx, G., et al. (2016). p120 Catenin-Mediated Stabilization of E-Cadherin Is Essential for Primitive Endoderm Specification. PLoS Genet. *12*, e1006243.

Pilauri, V., Bewley, M., Diep, C., and Hopper, J. (2005). Gal80 Dimerization and the Yeast GAL Gene Switch. Genetics *169*, 1903–1914.

Reynolds, A.B. (2007). p120-catenin: Past and present. Biochim. Biophys. Acta BBA - Mol. Cell Res. *1773*, 2–7.

Reynolds, A.B., Roesel, D.J., Kanner, S.B., and Parsons, J.T. (1989). Transformation-specific tyrosine phosphorylation of a novel cellular protein in chicken cells expressing oncogenic variants of the avian cellular src gene. Mol. Cell. Biol. *9*, 629–638.

Rodrigues, F.F., Shao, W., and Harris, T.J.C. (2016). The Arf GAP Asap promotes Arf1 function at the Golgi for cleavage furrow biosynthesis in Drosophila. Mol. Biol. Cell *27*, 3143–3155.

van Roy, F., and Berx, G. (2008). The cell-cell adhesion molecule E-cadherin. Cell. Mol. Life Sci. CMLS *65*, 3756–3788.

Sato, K., Watanabe, T., Wang, S., Kakeno, M., Matsuzawa, K., Matsui, T., Yokoi, K., Murase, K., Sugiyama, I., Ozawa, M., et al. (2011). Numb controls E-cadherin endocytosis through p120 catenin with aPKC. Mol. Biol. Cell *22*, 3103–3119.

Schwayer, C., Sikora, M., Slováková, J., Kardos, R., and Heisenberg, C.-P. (2016). Actin Rings of Power. Dev. Cell *37*, 493–506.

Shao, W., Wu, J., Chen, J., Lee, D.M., Tishkina, A., and Harris, T.J.C. (2010). A modifier screen for Bazooka/PAR-3 interacting genes in the Drosophila embryo epithelium. PloS One *5*, e9938.

Shapiro, L., and Weis, W.I. (2009). Structure and biochemistry of cadherins and catenins. Cold Spring Harb. Perspect. Biol. *1*, a003053.

Shibata, T., Kokubu, A., Sekine, S., Kanai, Y., and Hirohashi, S. (2004). Cytoplasmic p120ctn regulates the invasive phenotypes of E-cadherin-deficient breast cancer. Am. J. Pathol. *164*, 2269–2278.

Shimizu, T., Yabe, T., Muraoka, O., Yonemura, S., Aramaki, S., Hatta, K., Bae, Y.-K., Nojima, H., and Hibi, M. (2005). E-cadherin is required for gastrulation cell movements in zebrafish. Mech. Dev. *122*, 747–763.

Smythe, E., and Ayscough, K.R. (2006). Actin regulation in endocytosis. J Cell Sci *119*, 4589–4598.

Strutt, H., Gamage, J., and Strutt, D. (2016). Robust Asymmetric Localization of Planar Polarity Proteins Is Associated with Organization into Signalosome-like Domains of Variable Stoichiometry. Cell Rep. *17*, 2660–2671.

Takeichi, M. (1977). Functional correlation between cell adhesive properties and some cell surface proteins. J. Cell Biol. *75*, 464–474.

Thoreson, M.A., Anastasiadis, P.Z., Daniel, J.M., Ireton, R.C., Wheelock, M.J., Johnson, K.R., Hummingbird, D.K., and Reynolds, A.B. (2000). Selective Uncoupling of P120ctn from E-Cadherin Disrupts Strong Adhesion. J. Cell Biol. *148*, 189–202.

Toret, C.P., D'Ambrosio, M.V., Vale, R.D., Simon, M.A., and Nelson, W.J. (2014). A genome-wide screen identifies conserved protein hubs required for cadherin-mediated cell–cell adhesion. J Cell Biol *204*, 265–279.

Troyanovsky, R.B., Sokolov, E.P., Troyanovsky, S.M., and Nusrat, A. (2006). Endocytosis of Cadherin from Intracellular Junctions Is the Driving Force for Cadherin Adhesive Dimer Disassembly. Mol. Biol. Cell *17*, 3484–3493.

van de Ven, R.A.H., Tenhagen, M., Meuleman, W., van Riel, J.J.G., Schackmann, R.C.J., and Derksen, P.W.B. (2015). Nuclear p120-catenin regulates the anoikis resistance of mouse lobular breast cancer cells through Kaiso-dependent Wnt11 expression. Dis. Model. Mech. *8*, 373–384.

Wang, Y., Zhang, H., Shi, M., Liou, Y.-C., Lu, L., and Yu, F. (2017). Sec71 functions as a GEF for the small GTPase Arf1 to govern dendrite pruning of Drosophila sensory neurons. Development *144*, 1851–1862.

Wells, A., Yates, C., and Shepard, C.R. (2008). E-cadherin as an indicator of mesenchymal to epithelial reverting transitions during the metastatic seeding of disseminated carcinomas. Clin. Exp. Metastasis *25*, 621–628.

Figure 1. p120ctn levels determine the amount and dynamics of E-cad at the membrane. (**A-B**) Apical view of the dorsolateral epidermis of stage 15 *Drosophila* wild type embryos (**A-A'**) and *p120ctn*$^{-/-}$ mutant embryos (**B**) with cell outlines visualized by endogenously tagged E-cad-GFP. Two distinct cell borders exist: the longer Anterior-Posterior (AP, large arrow) and the short Dorsal-Ventral (DV, small arrow). (**A'**) Magnified image of the epidermal cells indicated in the box of (A), scale bar is 10 µm. (**C**) Quantification of the E-cad-GFP amount at the plasma membranes. (**D-D''**) Apical view of epidermis co-expressing *UAS::*p120ctn with *UAS::*CD8-Cherry using *en::*GAL4 with E-cad-GFP (green in D-D' and black in D'') and *UAS::*CD8-Cherry (magenta in D-D'). *UAS::*CD8-Cherry was used to mark cells expressing transgenes. (**D'-D''**) magnified micrograph of the region indicated in (D), scale bar is 10 µm. (**E**) Quantification of the E-cad-GFP amount at the plasma membrane in *UAS::*p120ctn and internal control. (**F**) Dynamics of E-cad-GFP measured by FRAP in the *UAS::*p120ctn. Average recovery curves (mean ± s.e.m.) and the best-fit curves (solid lines) are shown in F. All best-fit and membrane intensity data are in Supplementary Table S1. Bars in C and E represent difference between cell borders in genotypes measured by two-way ANOVA. *, $P < 0.05$; **, $P < 0.01$ ***, $P < 0.001$; ****, $P < 0.0001$. 10-20 embryos per genotype were used for intensity quantifications, and 8-10 embryos – for FRAP.

Figure 2. p120ctn regulation of E-cad is via the clathrin-mediated endocytic pathway. The localization of the clathrin light chain (*UAS::*CLC-GFP) in p120ctn mutant (*p120ctn*$^{-/-}$) embryos (**A-B**), and embryos overexpressing p120ctn (*UAS::*p120ctn) (**I-H**). **A** and **H** show the corresponding controls. Distinct puncta (spots, magenta in left images and black in right images) are observed at the membrane and in the cytoplasm. Cell outlines are visualized by anti-E-cad antibody staining (green in left images). Note that in control for p120ctn overexpression, there is additionally signal from *UAS*::CD8-mCherry in green. (**C-E** and **J-L**)

Quantification of the clathrin puncta in p120ctn mutant (*p120ctn*$^{-/-}$) embryos (**C-E**), and embryos overexpressing p120ctn (*UAS::*p120ctn) (**J-L**) by measuring the area (size, C and J), intensity (D and K), and the number (E and L) in control and p120ctn mutant. (**F** and **M**) The total amount of clathrin protein in these genotypes at the level of the adhesion junctions (AJs) obtained by multiplication of the puncta measurements. (**G** and **N**) FRAP of *UAS*::CLC-GFP in p120ctn mutant (G), and embryos overexpressing p120ctn (*UAS::*p120ctn) (N). Average recovery curves (mean ± s.e.m.) and the best-fit curves (solid lines) are shown in G and N. Statistical analysis is a two-tailed students t-test with Welch's correction. *, $P < 0.05$; **, $P < 0.01$ ***, $P < 0.001$; ****, $P < 0.0001$. 10-20 embryos per genotype were used for puncta quantifications, and 8-10 embryos – for FRAP.

Figure 3. p120ctn activates RhoA signalling at the plasma membrane.

(**A-B**) Apical view of the epidermis of control, p120ctn mutant (*p120ctn*$^{-/-}$) and p120ctn overexpression (*UAS::*p120ctn) embryos visualized with anti-E-cad antibody (**A**, grey in the left and middle images, green in the right image), *UAS*::CD8-mCherry (**A**, magenta in the right image, marks cells expressing *UAS::*p120ctn) and Rho-Kinase (Rok) tagged with Venus (**B**). (**C-D**) Quantification of Rok-Venus in the p120ctn mutant (**C**) and overexpressing embryos (**D**). (**E-F**) The epidermis of control, p120ctn mutant (*p120ctn*$^{-/-}$) and p120ctn overexpression (*UAS::*p120ctn) embryos visualized with anti-E-cad antibody (**A**, grey in the left and middle images, green in the right image), *UAS*::CD8-mCherry (**A**, magenta in the right image, marks cells expressing *UAS::*p120ctn), and Myosin II (MyoII) tagged with YFP (**F**). (**G-H**) Quantification of MyoII-YFP in the p120ctn mutant (**C**) and overexpressing embryos (**D**). Scale bars – 10 µm. Upper bars in **C, D, G** and **H** represent difference between genotypes and the lower - between cell borders measured by two-way ANOVA. *, $P < 0.05$; **, $P < 0.01$ ***, $P < 0.001$; ****, $P < 0.0001$. 10-20 embryos per genotype were quantified.

Figure 4. RhoA activity promotes the stabilization, and opposes the internalization, of E-cad at the membrane.

(**A-D**) Localization of E-cad in the epidermis following downregulation (the induction of Rho^{DN} expression for 4 hours, A-B) or upregulation (expression of Rho^{CA}, C-D, bottom images in C with top images being the corresponding control expressing *UAS*::CD8-Cherry alone) of Rho signalling. Cell borders are marked by E-cad-GFP (grey in left images, green in right images). Cells expressing transgenes are marked with an antibody for Engrailed directly (A) or by *UAS::*CD8-Cherry (C). Quantification of the E-cad-GFP at the membrane of the Rho^{DN} (B) or Rho^{CA} (D) expressing cells in comparison to internal control cells. The total amount of E-cad-GFP per cell upon upregulation of Rho signalling by Rho^{CA} expression is in Supplementary Fig. 3. (**E**) Localization of clathrin (*UAS*::CLC-GFP, grey in left images, magenta in right images) in cells co-expressing Rho^{CA} (bottom) and corresponding control co-expressing *UAS*::CD8-Cherry (top). Cell borders are visualized by anti-E-cad antibody staining (green in right images). (**F-H**) Quantification of the clathrin puncta area (F), intensity (G), and number (H) in the Rho^{CA} expressing cells. (**I**) FRAP of *UAS*::CLC-GFP in Rho^{CA} expressing cells. Average recovery curves (mean ± s.e.m.) and the best-fit curves (solid lines) are shown in I. Scale bars – 10 μm. *, $P < 0.05$; **, $P < 0.01$ ***, $P < 0.001$; ****, $P < 0.0001$. 10-20 embryos per genotype were used for puncta quantifications, and 8-10 embryos – for FRAP.

Figure 5. Arf1 is a downstream interactor of p120ctn.

Apical views of the epidermis expressing *UAS::*Arf1-GFP (Arf1, magenta in left images and grey in right images) with *en*::Gal4 in p120ctn mutant (*$p120ctn^{-/-}$*, **B**), embryos overexpressing p120ctn (*UAS*::p120ctn, **E**), and corresponding controls (**A** and **D**). Cell

outlines are visualized with anti-E-cad antibody staining (green in left images). The large *UAS*::Arf1-GFP puncta in the cytoplasm (large arrow in A) marks the Golgi (see Supplementary Fig. 3). The small arrow in A indicates the membrane resident population of Arf. (**C** and **F**) Quantification of the amount of *UAS::*Arf1-GFP at the plasma membrane between a control and p120ctn mutant (C), and control and p120ctn overexpressing (F) embryos. Scale bars – 10 μm. Upper bars in **C** and **F** represent difference between genotypes and the lower - between cell borders measured by two-way ANOVA. *, $P < 0.05$; **, $P < 0.01$ ***, $P < 0.001$; ****, $P < 0.0001$. 10-20 embryos per genotype were quantified.

Figure 6. Arf1 activity promotes the clathrin-mediated internalization of E-cad, and Arf1 overactivation rescues the defects in clathrin localization and dynamics in p120ctn mutant background.

Localization of E-cad (E-cad-GFP, **A**, grey in left image, and green in right image) and *UAS*::CLC-GFP (**C**, grey in left images, and green in right images) in cells expressing a dominant negative variant of Arf1 ($Arf1^{DN}$) with *en*::GAL4. Cell borders are visualized with E-cad-GFP (A) and anti-E-cad antibody staining (C, right image). *UAS*::CD8-Cherry was used to mark cells expressing $Arf1^{DN}$ in A (magenta, right image) and to balance the dose of GAL4-UAS (C, green, top images). (**B**) Quantification of the amount of E-cad-GFP at the plasma membranes of the $Arf1^{DN}$ cells compared to adjacent internal control cells. (**D**-**G**) Quantification of the *UAS*::CLC-GFP puncta area (D), intensity (E), number (F), and total protein content per cell (G, the product of the former three) in the plane of AJs in the $Arf1^{DN}$ cells. (**H**) Localization of *UAS*::CLC-GFP (grey in left images, magenta in right images) in *wt* control, expressing *UAS::*CLC-GFP alone (top images), and in embryos which are expressing a constitutively active Arf1 ($Arf1^{CA}$) in a p120ctn mutant ($p120ctn^{-/-}$) genetic background (bottom images). Cell borders were visualized with anti-E-cad antibody staining (green in

right images). (**I**-**L**) Quantification of the *UAS::*CLC-GFP puncta area (I), intensity (J), number (K), and total protein content per cell (L, the product of the former three) in the plane of AJs in the Arf1^{CA}; *p120ctn*$^{-/-}$ embryos. (**M**) FRAP of *UAS::*CLC-GFP in the plane of AJs in the Arf1^{CA}; *p120ctn*$^{-/-}$ embryos . Average recovery curves (mean ± s.e.m.) and the best-fit curves (solid lines) are shown in M. Scale bars – 10 µm. *, P < 0.05; **, P < 0.01 ***, P < 0.001; ****, P < 0.0001. 10-20 embryos per genotype were used for puncta quantifications, and 8-10 embryos – for FRAP.

Figure 7. RhoA signalling inhibits Arf1 and is independent of it.

(**A**) Localization of MyosinII-YFP (grey in left image) in the epidermis of cells expressing a constitutively active Arf1 (Arf1^{CA}) with *en*::GAL4 cells marked by *UAS::*CD8-Cherry (magenta in right image). Cell borders are visualized with anti-E-cad antibody staining (green in right image). (**B**) Quantification of the MyoII-YFP at the plasma membranes of the Arf1^{CA} cells and the adjacent internal control plasma membranes. (**C**-**D**) The localization of *UAS::*Arf1-GFP (grey in left images, magenta in right images) in control (**C)** and cells expressing RhoGEF2 RNAi (**D**). Large arrow indicates the Golgi resident Arf1 and the small arrow indicate the membrane resident population in **(C)**. Cell borders were visualized with anti-E-cad antibody staining (green in right images). (**E**) Quantification of the amount of *UAS::*Arf1-GFP at the plasma membranes of the RhoGEF2RNAi expressing cells. Scale bars – 10 µm. *, P < 0.05; **, P < 0.01 ***, P < 0.001; ****, P < 0.0001. 10-20 embryos per genotype were quantified.

Figure 8. p120ctn increases the tension at the plasma membrane, and the model of p120ctn action.

(**A**) Examples of laser ablation in epidermal cells in control (top images), p120ctn mutant (*p120ctn*$^{-/-}$, middle images), and p120ctn overexpressing (*UAS*::p120ctn, bottom images). Cells shown immediately before (left images) and after ablation (right images). Cell borders are visualized with E-cad-GFP (grey). The small arrows indicate the connected vertices of the ablated membrane used to measure distance during the course of the experiment. The large arrows on the post-ablation images represent the position at which the microablation was performed, for which a small spot of discolouration can be observed. (**B**) Quantification of the initial recoil of the ablated membranes, expressed as a percentage increase in distance relative to the length of the membrane prior to ablation. **(C)** Model of the interaction between p120ctn, RhoA, Arf1, clathrin, and actin. In normal conditions p120ctn acts on both Arf1 and RhoA signalling pathways: Rho promotes the stabilization of E-cad at the plasma membrane and Arf1 promotes E-cad internalization by recruiting clathrin. RhoA additionally inhibits Arf1, possibly directly (dashed red lines) or indirectly by increasing the density of the cortical actin. (**C'**) Overexpression of p120ctn leads to overactivation of the Rho signalling pathway, resulting in an increase in cortical actin and indirect suppression of Arf1 signalling. Overall this results in an increase in E-cad amount and stability at the membrane. (**C"**) Conversely in the absence of p120ctn both the Rho and Arf1 pathways are not stimulated. Therefore, both cortical actin tension and clathrin mediated endocytosis are reduced. The lower levels of E-cad at the membrane result from the reduction of recycling and actin mediated stabilization by p120ctn. Scale bar – 10μm. *, $P < 0.05$; **, $P < 0.01$ ***, $P < 0.001$; ****, $P < 0.0001$. 14-20 embryos per genotype.

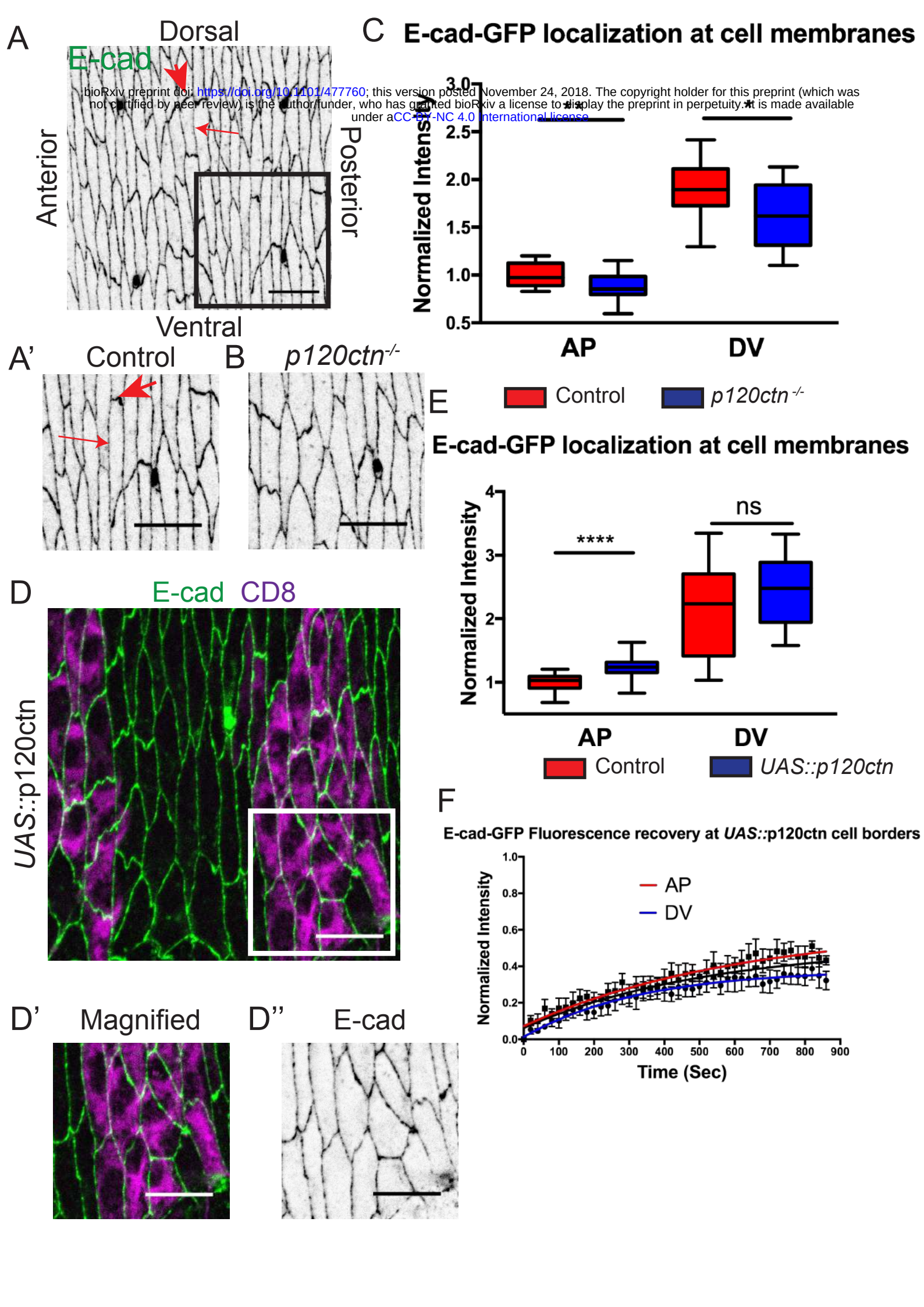

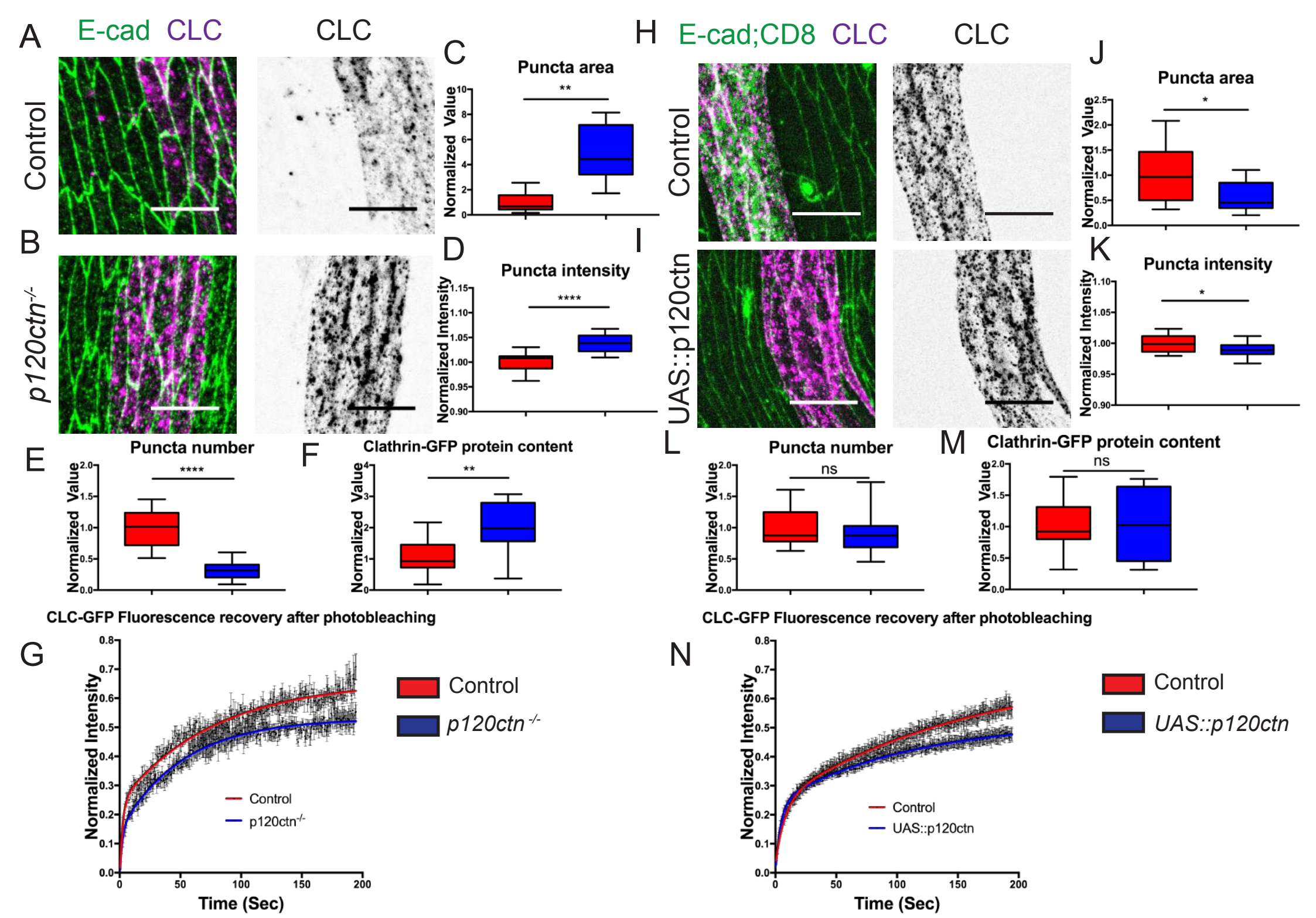
A
E-cad CLC
CLC
Control
B
p120ctn-/-
C
Puncta area
**
Normalized Value
D
Puncta intensity
****
Normalized Intensity
H
E-cad;CD8 CLC
CLC
Control
I
UAS::p120ctn
J
Puncta area
*
Normalized Value
K
Puncta intensity
*
Normalized Intensity
E
Puncta number
****
Normalized Value
F
Clathrin-GFP protein content
**
Normalized Value
L
Puncta number
ns
Normalized Value
M
Clathrin-GFP protein content
ns
Normalized Value
CLC-GFP Fluorescence recovery after photobleaching
G
Normalized Intensity
Time (Sec)
Control
p120ctn-/-
CLC-GFP Fluorescence recovery after photobleaching
N
Normalized Intensity
Time (Sec)
Control
UAS::p120ctn

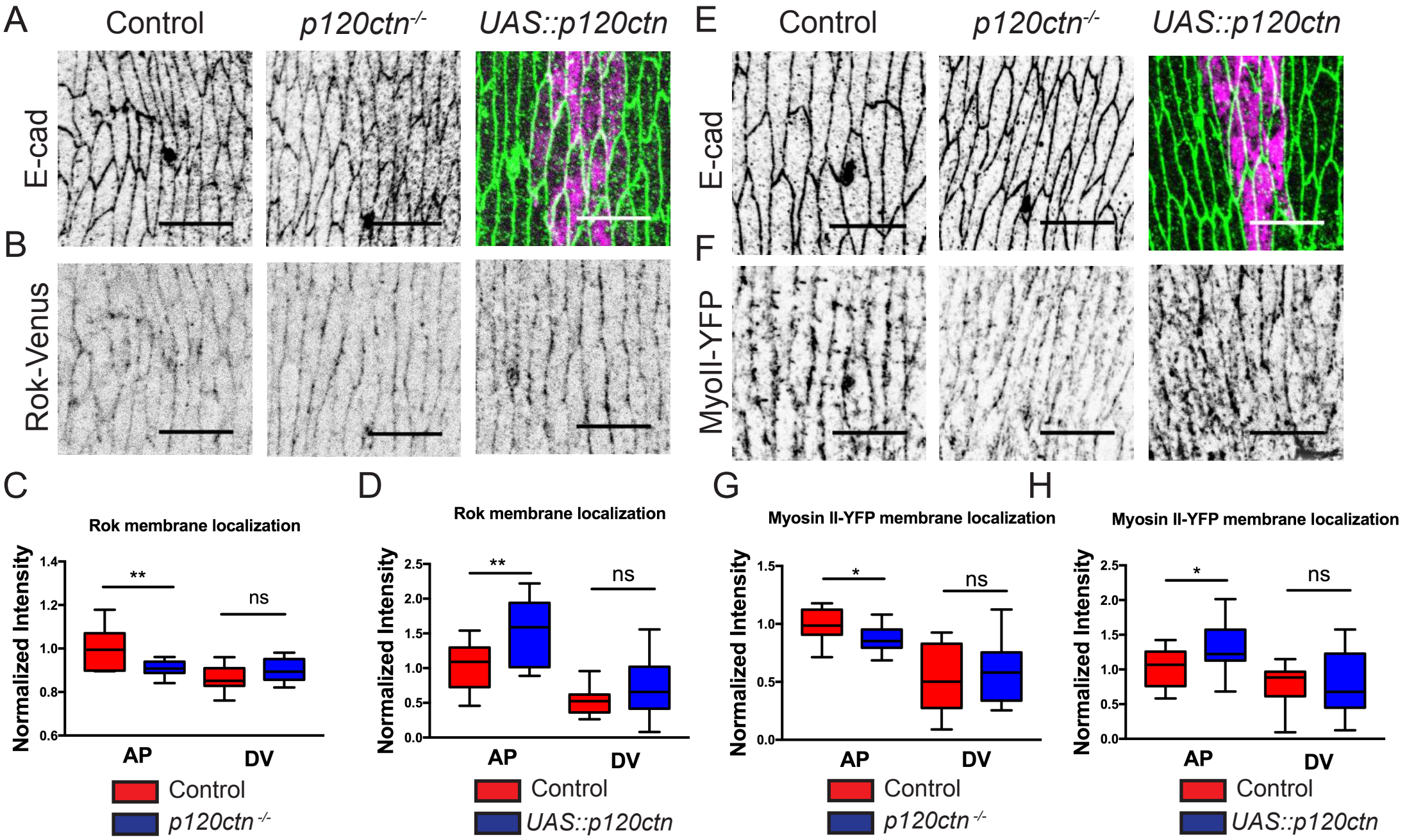
A
Control
p120ctn-/-
UAS::p120ctn
E-cad
B
Rok-Venus
E
Control
p120ctn-/-
UAS::p120ctn
E-cad
F
MyoII-YFP
C
Rok membrane localization
Normalized Intensity
1.4
1.2
1.0
0.8
0.6
**
ns
AP
DV
Control
p120ctn -/-
D
Rok membrane localization
Normalized Intensity
2.5
2.0
1.5
1.0
0.5
0.0
**
ns
AP
DV
Control
UAS::p120ctn
G
Myosin II-YFP membrane localization
Normalized Intensity
1.5
1.0
0.5
0.0
*
ns
AP
DV
Control
p120ctn -/-
H
Myosin II-YFP membrane localization
Normalized Intensity
2.5
2.0
1.5
1.0
0.5
0.0
*
ns
AP
DV
Control
UAS::p120ctn

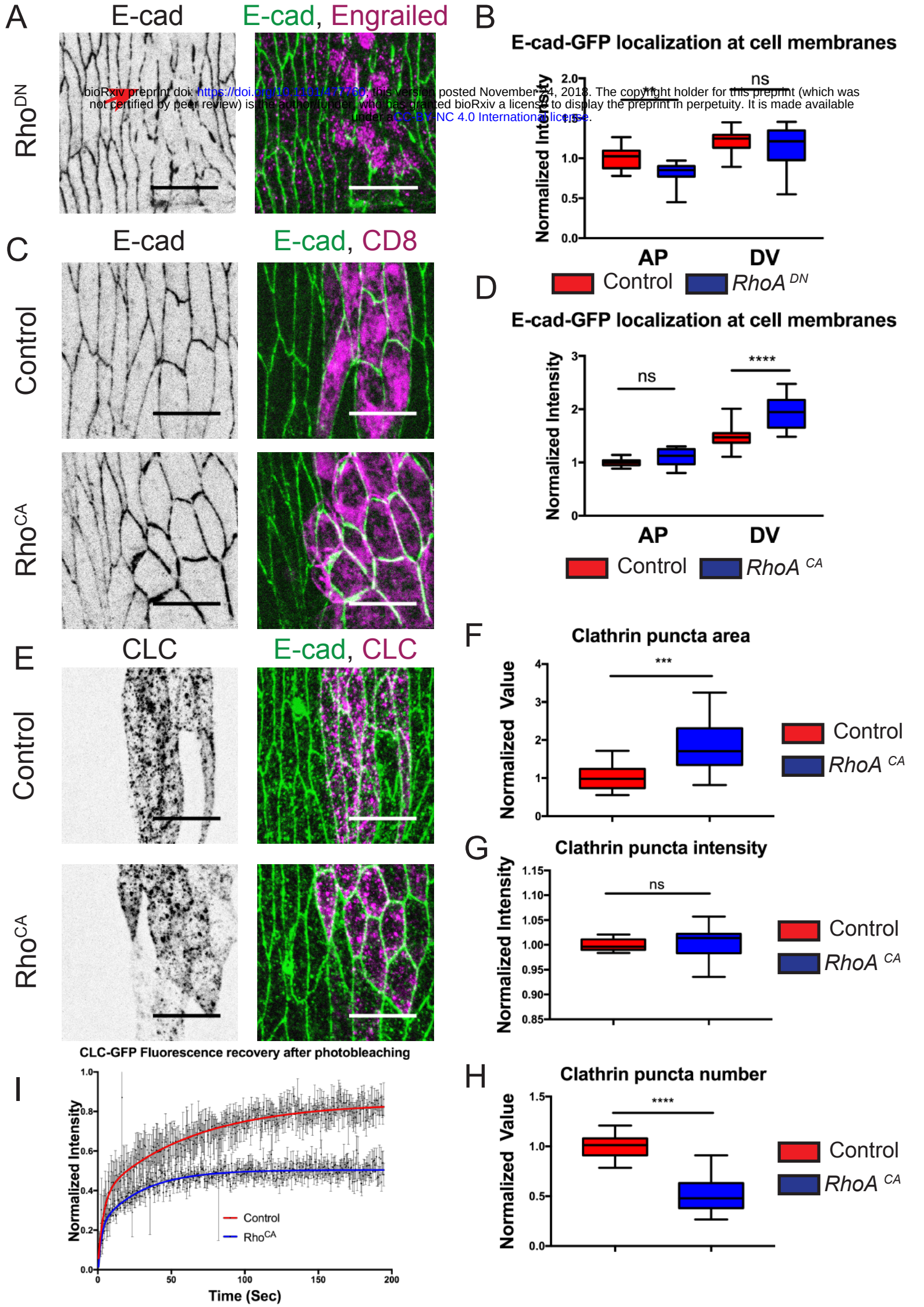

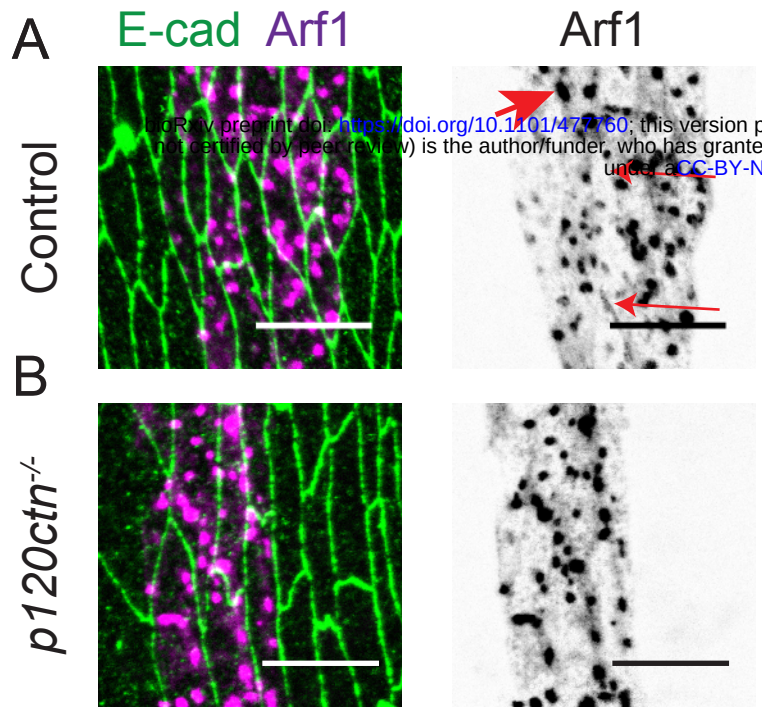

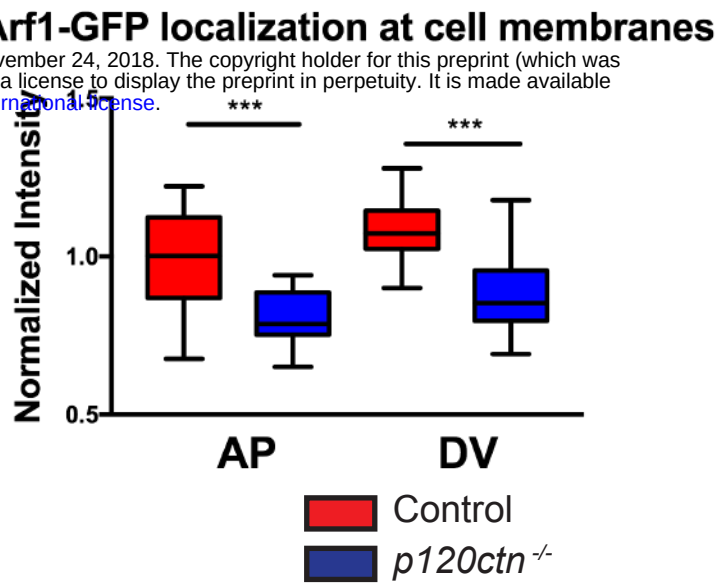

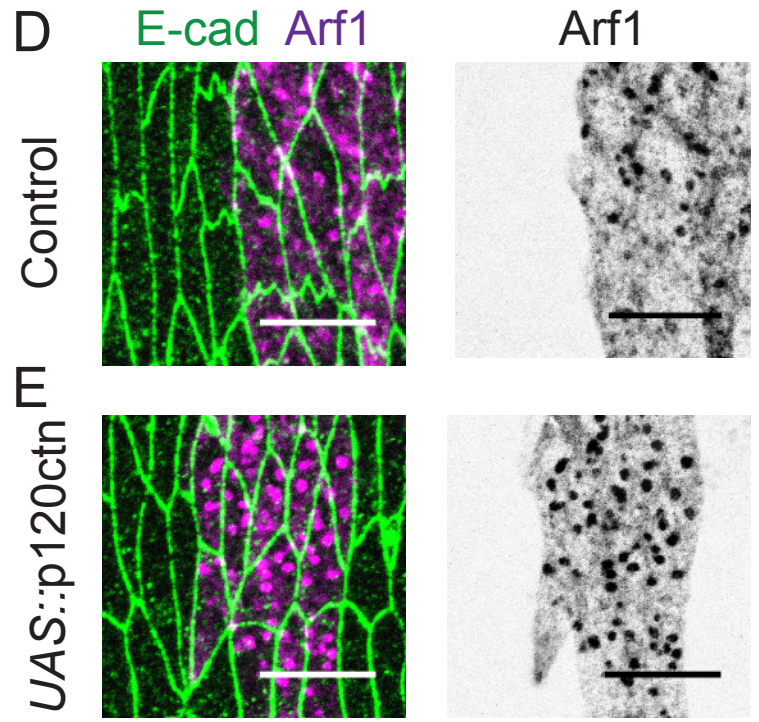

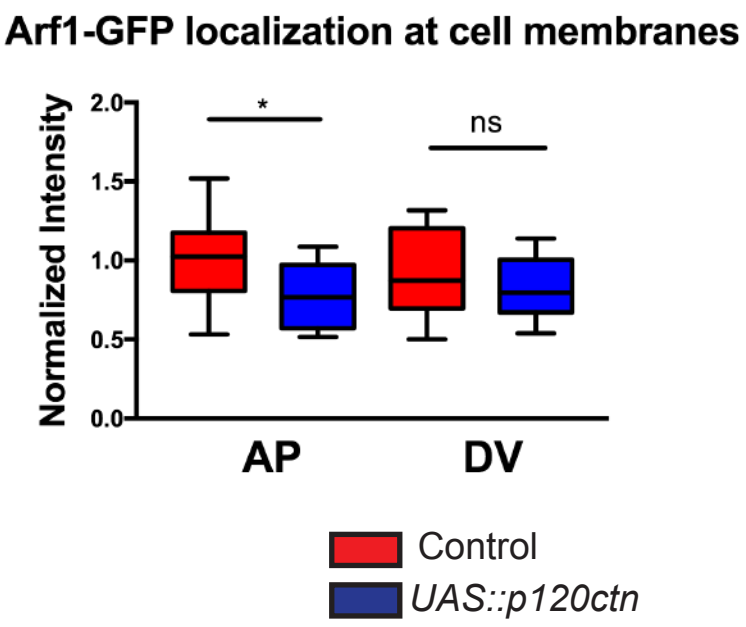

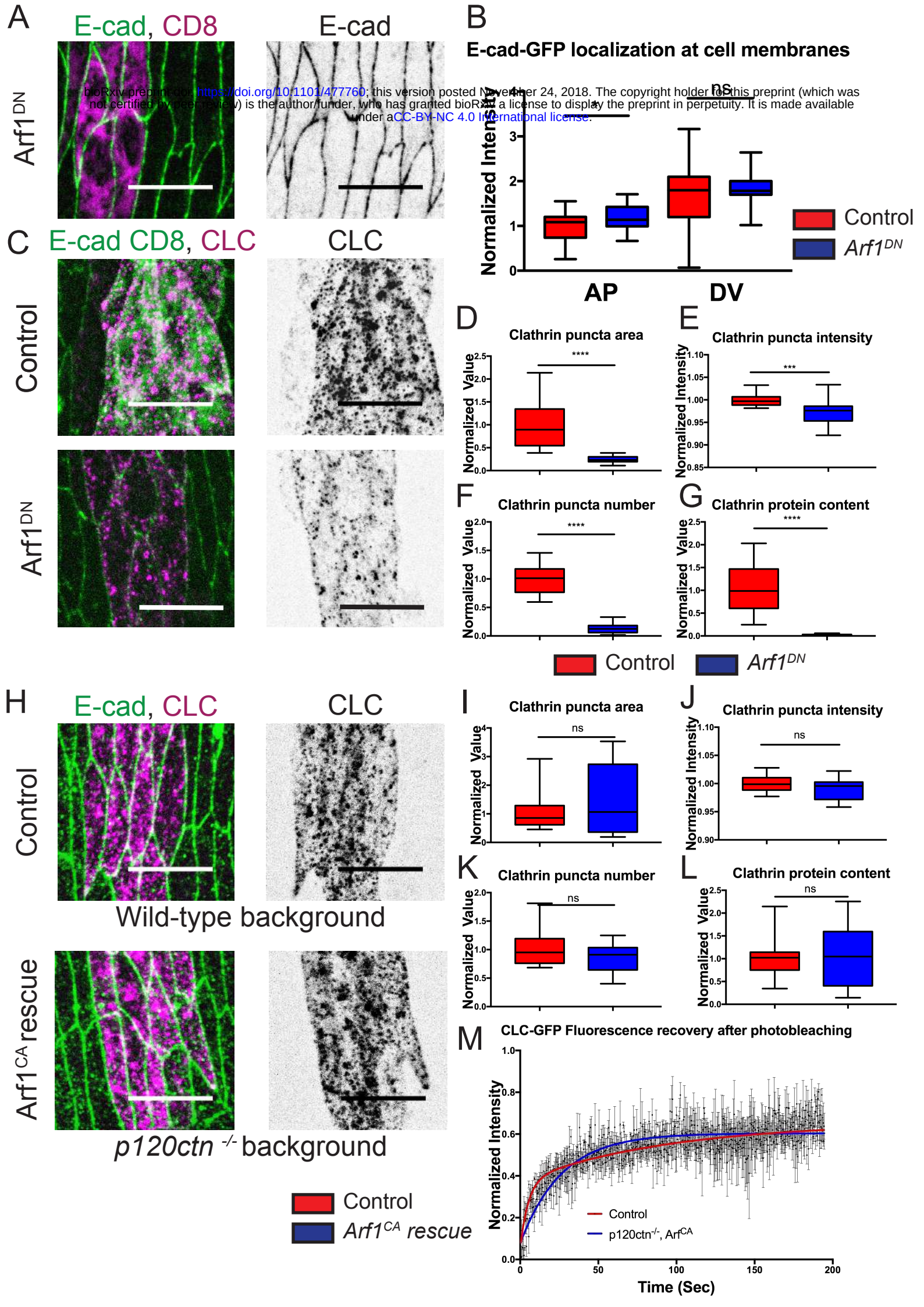

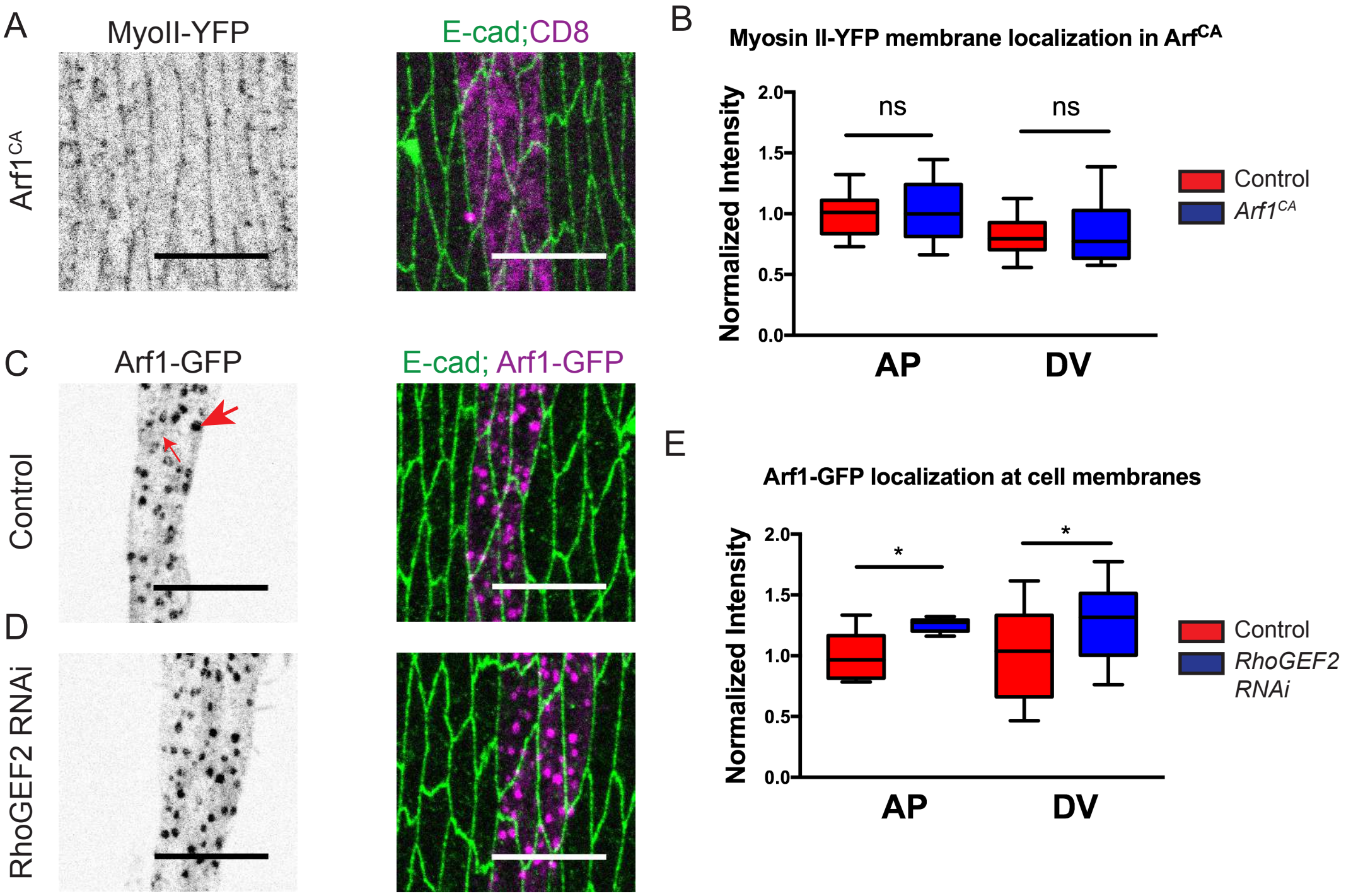
A
MyoII-YFP
E-cad;CD8
Arf1CA
B
Myosin II-YFP membrane localization in ArfCA
Normalized Intensity
2.0
1.5
1.0
0.5
0.0
ns
ns
AP
DV
Control
Arf1CA
C
Arf1-GFP
E-cad; Arf1-GFP
Control
D
RhoGEF2 RNAi
E
Arf1-GFP localization at cell membranes
Normalized Intensity
2.0
1.5
1.0
0.5
0.0
*
*
AP
DV
Control
RhoGEF2
RNAi

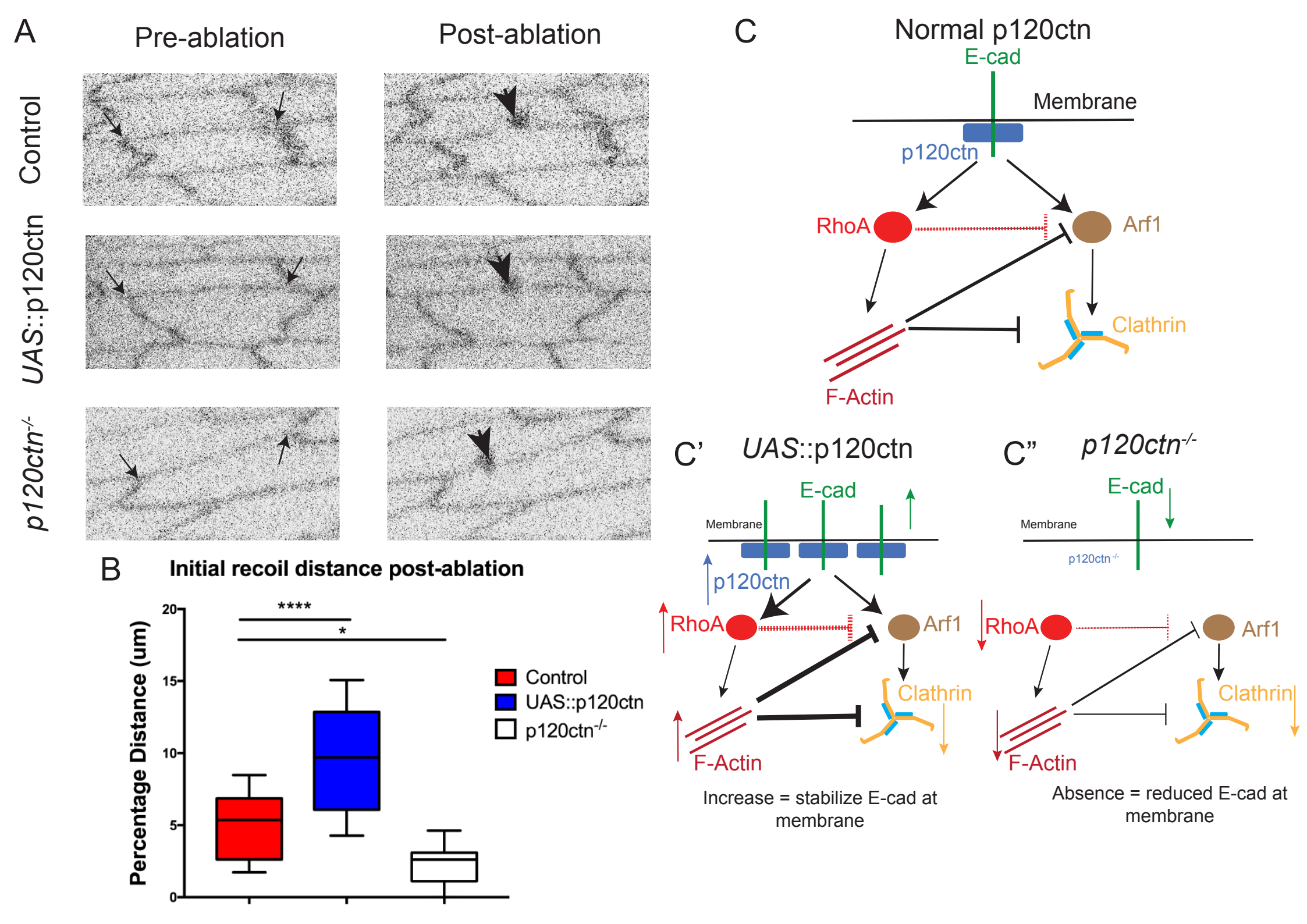
A
Pre-ablation
Post-ablation
Control
UAS::p120ctn
p120ctn-/-
B
Initial recoil distance post-ablation
Percentage Distance (um)
20
15
10
5
0
****
*
Control
UAS::p120ctn
p120ctn-/-
C
Normal p120ctn
E-cad
Membrane
p120ctn
RhoA
Arf1
Clathrin
F-Actin
C'
UAS::p120ctn
E-cad
Membrane
p120ctn
RhoA
Arf1
Clathrin
F-Actin
Increase = stabilize E-cad at membrane
C"
p120ctn-/-
E-cad
Membrane
p120ctn-/-
RhoA
Arf1
Clathrin
F-Actin
Absence = reduced E-cad at membrane